LOAD MONITOR 1

REPORT 2018:482

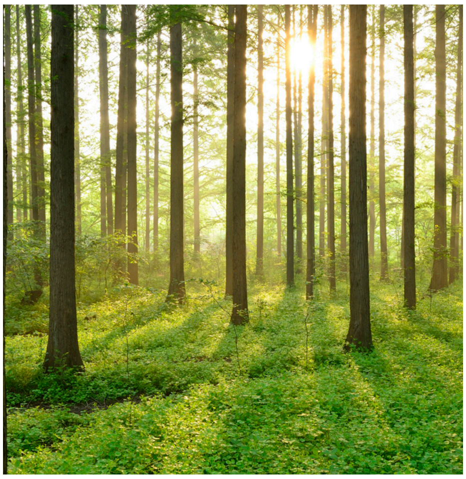


Load Monitor 1

Measuring and modeling vibrations and loads on wind turbines

JOHANNES LINDVALL, UTKU TURKYILMAZ, JOHAN HANSSON, INGEMAR CARLÉN, STEFAN IVANELL, HUGO OLIVARES-ESPINOSA, JOHAN ARNQVIST

ISBN 978-91-7673-482-7 | © Energiforsk June 2018

Energiforsk AB | Phone: 08-677 25 30 | E-mail: kontakt@energiforsk.se | www.energiforsk.se

Förord

LoadMonitor – Mätning och modellering av vibrationer och laster på vindkraftverk" är ett projekt finansierat av Energiforsk och Energimyndigheten genom programmet Vindforsk IV.

Projektets övergripande mål är att öka kunskapen om hur turbinlaster och turbinprestanda påverkas av svenska klimat-, skogs och terrängförhållanden.

Med hjälp av nacellemonterad lidar, SCADA systemet och ett egenutvecklat vibrationsmätningssystem har man dels undersökt kopplingen mellan den ostörda vinden och vibrationer i nacellen (del 1) och dels hur man på ett kostnadseffektivt sätt kan mäta laster i strukturen (del 2). Sist men inte minst har man genom projektet fått möjlighet att validera en strömningsmodell över skog som är av stort värde då en stor del av den svenska vindkraften är placerad i skog.

Projektet har utförts av Kjeller Vindteknikk, Uppsala Universitet campus Gotland och Teknikgruppen med stöd av Stena Renewable.

Göran Dalén

Ordförande, Vindforsk IV

Sammanfattning

Målet med denna studie är ökad kunskap om hur turbinlaster och turbinprestanda påverkas av svenska klimat-, skogs och terrängförhållanden.

Projektet bygger på ett mätprogram som inkluderar högfrekvent data från nacellemonterad lidar, SCADA systemet, ett egenutvecklat vibrationsmätningssystem och simulerad atmosfärisk stabilitet.

Slutrapporteringen LoadMonitor-projektet är uppdelad i två parallella rapporter. Denna rapport (huvudrapporten) täcker analysen av data från LoadMonitorsajten. Analysen har delats upp i tre delar:

- Att relatera inkommande vindkarakteristik till nacellevibrationer
- Att relatera inkommande vindkarakteristik och nacellevibrationer till turbinprestanda
- Vidareutveckla och validera en flödesmodell till att representera parkområdets heterogena yta (terräng och växtlighet)

I den parallella rapporten är fokus på olika koncept för övervakning av laster på vindkraftverk. System för att underlätta sådan övervakning har utvecklats inom projektet och presenteras detaljerat i den rapporten.

De huvudsakliga slutsatserna från denna rapport.

Vi hittar inga tydliga relationer mellan atmosfärens tillstånd (vindförhållande och atmosfärisk stabilitet) och vibrationerna i nacellen. Det finns indikationer på att vibrationerna ökar med ökad vindhastighet, ett samband som försvagas med ökad atmosfärisk stabilitet. En grundligare analys än den genomförda kan potentiellt visa på tydligare samband.

Den relativa produktionseffektiviteten avtar starkt med ökad atmosfärisk stabilitet. Dämpning av turbulens associerad med ökad atmosfärisk stabilitet verkar var den huvudsakliga förklaringen till detta. Det bör poängteras att den analyserade perioden domineras av relativt låga vindhastigheter och att enbart ett fåtal episoder med vindar runt/över vindnivån som ger max effekt är representerade.

Strömningsmodellen, som modifierats för att kunna modellera heterogen skog och terräng, validerades med lyckat resultat för tillfällen med neutral atmosfärisk stabilitet i en vindriktning utan störningar från uppströms turbiner. Valideringen av modellen görs mot vindprofiler och vindhastighetsfördelningar uppmätta av den nacellemonterade lidarn för olika uppströms positioner. Att modellen klarar att reproducera strömningen ovan en heterogen skog med topografi är ett stort steg mot tillförlitliga simuleringar av vakinteraktioner inom landbaserade vindkraftsparker.

Summary

This study aims to increase our knowledge on how climate, terrain and forest conditions corresponding to those of Sweden affects the performance of, and loads on a wind turbine.

The backbone of the project is a measurement program which includes nacelle mounted lidar, tower vibration measurements, SCADA output and simulated atmospheric stability, all with a high temporal resolution.

The LoadMonitor reporting is divided into two parallel reports. This report (the main report) covers the analysis of the data collected at the LoadMonitor site. The focus of the analysis is threefold:

- Relate upstream wind conditions to tower top vibrations
- Relate upstream wind conditions and tower top vibrations to turbine vibrations
- Development and validation of a flow model that represents the site specific heterogeneous canopy and varying topography.

In the parallel report focus instead is on concepts for monitor loads on wind turbine towers and foundations. Systems to facilitate such monitoring have been developed in the project and are presented in detail in that report.

Regarding the main conclusions in this report:

No strong relationships between the ambient conditions (wind and thermal stratification) and the vibration levels are found in our analysis. There are indications that the vibrations increase with increasing wind speeds, a relationship that becomes less pronounced with increased atmospheric stability. A more thoroughly analysis of the data would potentially result in stronger relationships.

The relative production efficiency decreases rather strongly with increasing atmospheric stability. Suppression of turbulence with increasing atmospheric stability seems to be the main explanation. It should be noted that the analyzed period is dominated by relatively low wind speeds and that wind speeds near the rated wind speeds were rare.

The flow model, modified to represent the non-homogenous local variations in canopy density and terrain, was capable of reproducing both the mean wind profiles at different upstream positions and the corresponding probability distributions of velocity fluctuation as measured by the nacelle mounted lidar for neutral and wake-free conditions. The fact that the flow model can reproduce the wind field over forest is a large step towards an accurate computation of wake interaction inside wind farms.

List of content

1 Introduction

Optimized operation and maintenance of wind turbines is a topic of large interest within research and development. The main goal is to maximize turbine energy availability while maintaining loads below reasonable limits. This report will not provide a full methodology for turbine operation and load optimization, but rather some pieces that will be relevant for the understanding of how turbines respond to different ambient conditions.

The relation between the upstream wind characteristics and nacelle vibrations is analyzed based on concurrent 3D-measurements of the upstream wind and high resolution vibration measurements. Based on these measurements, the study aims to give new insights to the relation between the wind gradient and turbulence of the upstream wind to the nacelle vibrations and the resultant loads on the wind turbine.

One of the main goals of LoadMonitor was to set up a combined measurement and analysis system that facilitates to detect underperformance and identify non-standard wind conditions and component failures. The combined measurement program consists of measurements of nacelle vibrations, upstream wind conditions and SCADA data, all with high temporal resolution. In addition the combined measurements will be used to validate state-of-the art large-eddy-simulations of the wind farm. The knowledge and tools developed within this project will be of high relevance for turbine performance control since the project resulted in increased flow model accuracy and a methodology to study vibrations of turbines located in complex sites.

The main objectives of the LoadMonitor project are

- Present conclusions about the relationship between turbine performance and wind shear, inflow angle (horizontal) and turbulence.
- Measure the up-stream wind conditions with a nacelle based lidar
- Develop a portable, stand alone, sensor to measure nacelle vibrations with high temporal resolution and high accuracy down to low frequencies.
- Provide gained knowledge about the relationship between turbine performance and nacelle vibrations.
- Present a methodology for identification of underperformance by analysis of measured vibrations.
- Present a methodology to quantify load levels (fatigue) in important components by analysis of measured nacelle vibrations and analysis of SCADA data.
- Present a description of the relationship between the nacelle vibrations and relevant parameters describing the up-stream wind flow: wind speed, wind shear, horizontal inflow angle and turbulence.
- Report about the validation of the state-of-the art calculations of wake losses based on the measurements.

1.1 MOTIVATION

The power curve is a standard way to define the electrical power produced by a wind turbine as a function of air density and wind speed. However, a standard power curve does not give a complete description of the performance of a wind turbine during different wind shear and turbulence conditions. Ongoing studies performed in an international collaboration between project developers, turbine manufacturers, consulting companies and academic institutions, called "Power Curve Working Group, (PCWG)", have presented new parameters and methodologies (e.g. "rotor equivalent wind speed", "turbulence (re)normalization methods") in an attempt to better describe how the produced power depends on the turbulence and wind shear across the whole rotor (PCWG-1, 2016) . The group is also discussing the possibility to replace the power curve with an "electrical vs. kinetic power"-curve, and wind measurements with kinetic energy measurements. The aim is to provide a more complete description of how the energy in the wind across the whole rotor is converted into electrical energy.

Further knowledge about the performance of a wind turbine during different wind shear conditions and turbulence levels is relevant material for site suitability studies and discussions regarding the warranted power curve and turbine performance. In addition, there is a need for tools making it possible to identify for which conditions wind turbines that are performing less than expected, and understanding the underlying causes.

The main purpose of the LoadMonitor project is to present a combined measurement and analysis system that measure and log turbine motions with high temporal resolution. These measurements are analyzed with SCADA parameters to investigate the performance of the turbine, and to identify causes of underperformance (if any), such as non-standard wind conditions and/or possible defect components.

The instrument measuring vibrations is small and stand-alone, easily installed in the nacelle, measuring nacelle vibrations with high temporal resolution (50 Hz was used during the measurement campaign) and with high precision. Concurrent measurements of parameters characterizing the up-stream wind flow, e.g. wind speed, wind shear, and turbulence will be made and related to the measured vibrations. The aim is to identify the signatures of different wind shear and turbulence conditions in the measured motion signals and relate them to the turbine performance. Based on this, the combined measurement and analysis system will be used on other operational wind turbines as a tool to identify underperformance and to understand the underlying causes.

In addition, the project creates a unique opportunity to verify the state-of-the-art calculations of loads and wake losses. Nacelle based lidar wind measurements will be made on two nearby turbines simultaneously, providing material for validation of wake and load models. Within the Nordic consortium "Optimization of large wind farms" (Ivanell, et al., 2013), wakes and their influence on production and loads are studied. The purpose is to gain deeper understanding of wake propagation and loads caused by the wakes to optimize the layout and operation of wind farms. LoadMonitor will give the possibility to compare the modelled results with the measured wind conditions.

1.2 PROJECT SETUP AND FINAL REPORT CONTENT

LoadMonitor is a collaboration between Kjeller Vindteknikk AB (KVT), Teknikgruppen AB (TG), Uppsala University Campus Gotland (UUCG), Stena Renewable (Wind farm owner) (SR), and Zephir Lidar (lidar manufacturer) (ZP). Kjeller Vindteknikk is managing the project.

The final reporting of the LoadMonitor project consists of two reports. This report, which should be considered as the main report, analyzes the measurements and simulations of the LoadMonitor site, a forested wind farm in southern Sweden. In a parallel second report (Carlén, 2017) vibration measurement, SCADA data, load measurements and aerolastic simulations of the Ryningsnäs wind farm are combined to find relationships between the vibrations and loads.

The chapters and the main authors are summarized in Table 1.1. The modelling of wake losses is still on-going work. The improvement in the large eddy simulation-model (LES) in terms of representing forest heterogeneities and topography of the LoadMonitor site is presented in this report, while results from merging the LES-model with a wake model and comparing with LoadMonitor measurements will be subject to future publications. Conclusions and future work is presented in Chapter 3, Chapter 4 and in the Ryningsnäs Report (Carlén, 2017).

Table 1.1. Overview of main responsibilities

Chapter	Responsible
Main report Ch 2.1-2.2,2.5-2.6 and 3	KVT
Main report Ch. 2.4 and 4	UUCG
Main report Ch. 2.3 and Ryningsnäs Report	TG

2 Description of measurements and numerical models used in the project

Measurements have been made with two nacelle mounted lidars on two different turbines, and with an instrument for measuring vibrations in one of these turbines. The latter instrument is developed in the project. In addition SCADA data from the wind farm and reference data from a numerical model has been available in the project. A time line showing the availability of the data is found in Figure 2-1. The data is described in more detail in the following sections. The analysis in this report only utilizes data from the ZephirDM nacelle lidar, data from the Wind Iris is planned to be used in a forthcoming wake study mentioned in Sect. 4.3.

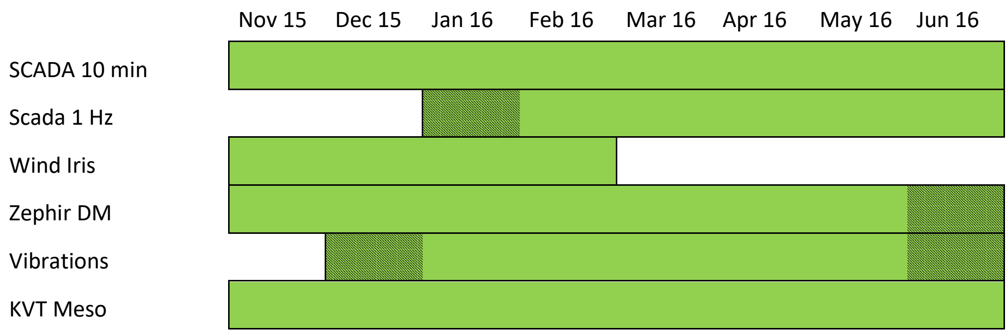

Figure 2-1: Time line showing the data that is available in the project. Hatched months indicate that data is only available for part of the months.

2.1 WIND IRIS

Wind Iris (WI), a nacelle mounted 2-beam forward-looking pulsed type of lidar, has been used in this research project. The WI was previously used in the Energiforsk project ProdOptimize (Lindvall et al., 2016; Turkyilmaz & Undheim, 2016; Hansson et al., 2016) and without major costs the measurement could be extended to cover parts of the LoadMonitor period. WI measures the horizontal wind speed, and the horizontal wind direction relative to the WI orientation, at 10 ranges (R1 to R10) upstream of the turbine. The measurements are based on two horizontal lidar beams separated by a horizontal opening angle (30° in this WI configuration) centred along the roll axis of the system. The horizontal wind speed and direction are derived from the radial speeds measured along the line of sight (LOS) of each beam assuming horizontally homogeneous wind flow. The data is recorded both as real time data (1 sec resolution) and as 10 min averaged data.

Table 2.1 summarizes the main configuration parameters used in this research project.

Table 2.1 Main configuration parameters of the WI system used in this research project.

Parameter	Description
Measurement ranges	80, 120, 160, 200, 240, 240 280, 320, 360, 400, 440 m
Probed length	60 m
Number of measurement distances	10
Laser source	Fiber pulsed laser 1.54 µm
Opening angle	15 ° (α: half angle)
Acquisition frequency	1 Hz
CNR Noise threshold	- 23 dB

2.1.1 Description of data measured by the Wind Iris

As described the WI data is available as both real time data (1 sec resolution) and average (10 min) data. The analyses are based on the 10-min average values of the following main WI parameters available at 10 distance ranges:

- **Horizontal wind speed (HWS):** reconstructed from radial wind speeds on each LOS with standard deviations
- **Relative wind direction (directionm):** calculated from radial wind speeds on each LOS with standard deviations
- **HWS availability (HWSa):** defined as the percentage of valid 1 sec measurements used to calculate the 10 min average values of the HWS.

In addition below parameters are also available:

- **Carrier to Noise Ratio (CNR):** in order to check the quality of measurements (its threshold set to -23 dB)
- **Tilt and roll angles:** measured by WI's internal sensors, used in alignment of WI and estimating height of measurements at each measurement range.

Moreover there is also turbulence intensity data available from WI that is derived from standard deviation of wind speed measurements.

2.1.2 Measurement campaign information:

The last measurement campaign of ProdOptimize research project (WF2 WT07) has been continued in this research project (Turkyilmaz & Undheim, 2016). The installation of Wind Iris was performed by Kjeller Vindteknikk with the support of Avent Lidar Technology and wind turbine manufacturers' service team members. The details of the installation procedures and measures are explained in the report of ProdOptimize research project (Turkyilmaz & Undheim, 2016).

2.2 ZEPHIR DM

In this research project a Zephir Dual Mode (ZDM) nacelle mounted continuous wave (CV) lidar have been used. The ZDM measures the LOS wind speed at 50 points around a circular scan each second upwind of the turbine. Based on the LOS data a multitude of wind related parameters is calculated assuming horizontally homogeneous wind flow. The parameters are described in section 2.2.1.

Measurements can be made at multiple ranges. The ranges have been changed during the project due to different requirements on the data for different tasks. In addition to the ranges it is also possible to divide the scanning cone in horizontal segments as shown in Figure 2-2. The parameters calculated for each segments is described in section 2.2.1.

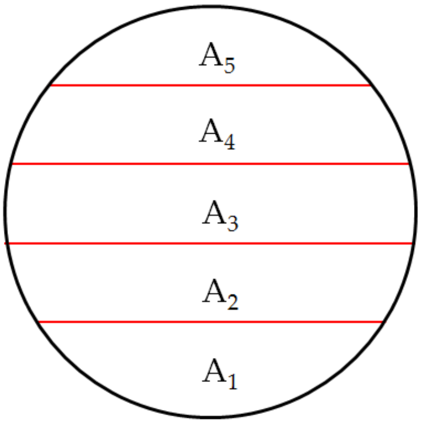

Figure 2-2: The black line represents the scanning circle of the ZDM. The circle can be divided into segments where the measurement points on both sides of the segment are used to calculate different parameters.

The half angle of the scanning cone is fixed at 15º. The data is recorded as

- raw data with recordings for each point on the circle
- 1 second values
- 10 minute average values

The three configurations used in ZephIR DM are summarized with timeline in Table 2.2 and with parameter settings in Table 2.3.

Table 2.2 Timeline of the main configurations of ZephIR DM used in this research project.

	Nov 15	Dec 15	Jan 16	Feb 16	Mar 16	Apr 16	May 16	Jun 16
Config 1								
Config 2								
Config 3								

Table 2.3 Configuration parameters of the ZephIR DM used in this research project.

Parameter	Measurement ranges	Revs per range	Number of rotor slices
Config 1	300 m, 263 m, 211 m, 160 m, 108 m, 57 m, 10 m	5	13
Config 2	300 m x 3, 211 m x 3, 108 m x 3, 10 m	60	5
Config 3	200 m x 9, 10 m	60	5

2.2.1 Description of data measured by the Zephir DM

As mentioned, the ZDM is measuring the LOS wind speed on 50 points around the edge of the scanning circle. The LOS measurements are the basis for the derivation of the wind speed for different parts of the rotor plane.

Raw data

It is about 20 ms between adjacent recordings in the raw data files. For each time step information about the inclination, roll and fore-aft velocity of the ZDM is recorded. The raw files also contain information about the presence of rain and the LOS wind speed for each point. There is also information about the reflected signal in the form of spectrums.

1 s data

The files with 1 s data contain basic information about roll and inclination, status of the system, and GPS position. The meteorological variables available in the files consists of

- Data from the meteorological station mounted on the ZDM (wind, pressure, humidity, rain, tilt, compass direction)
- Variables from the Fit Derived (FD) algorithm. The FD algorithm fits a function to all points on the scanning circle to calculate the yaw misalignment, the horizontal wind speed at the scan centre, the vertical wind shear exponent, and the horizontal wind speed at hub height.
- LOS wind speed from the left and right side of the defined segments over the scanning circle

10 minute average date

The files with 10 minute average data contain basic information about roll and inclination, status of the system, and GPS position. The meteorological variables available in the files consists of

- Data from the meteorological station mounted on the ZDM as for the 1 s data but with additional information about standard deviation for some of the variables.
- Variables from the FD algorithm as for the 1 s data but with additional information about standard deviation for some of the variables.
- Variables from the Pair Derived (PD) algorithm. The PD algorithm makes use of the left and right LOS on each defined segment of the rotor to calculate the horizontal wind speed, the yaw misalignment, and turbulence intensity on

each segment. Based on the results from the PD algorithm the Rotor-Equivalent-WindSpeed (REQWS) is also calculated

2.2.2 Measurement campaign information

The installations were performed by Kjeller Vindteknikk, Zephir Limited and wind turbine manufacturers' service team members. The configuration changes explained in the previous chapter were applied via remote access to the lidar.

The alignment of the lidar during the installation was done by using Waltz Software's real-time inclination and roll setup. Both quantities are measured with built in accelerometers and the mechanical adjustments were made in the assembly until acceptable values were achieved. The yaw alignment of the lidar was performed with an alignment laser available from ZDM. A reference line parallel to the rotor axis and a bolt point on top of the gear box, seen from the nacelle roof through the open hatch, were used to perform the alignment. In addition, a post installation validation was made by using the blade reflection plot (so called figure of eight) available in Waltz Software, in order to ensure that the figure is centred by the symmetry axis.

The network communications were made with a 3G modem. The data access and monitoring, time synchronization and ftp connections were made with ZDM's software Waltz.

Figure 2-3: Installed ZephIR DM on the wind turbine nacelle (photos courtesy of Kjeller Vindteknikk)

2.2.3 Height of measurements

As the terrain is not flat, the height of measurement will differ depending on the nacelle yaw angle, see Figure 2-14. The wind follows the terrain and the different heights of measurement can have an impact on the measurements. No correction for this is applied on the data in the analysis unless stated otherwise in the text.

2.2.4 Site calibration

If a power curve validation should be made on this turbine at this site, a site calibration would be necessary according to (IEC 61400-1, 2005). No site calibration has been made in the current project.

2.3 VIBRATIONS

Accurate and robust wind turbine nacelle acceleration signals are useful for various purposes depending on the situation. The main use is to serve as an important component of the turbine safety system, where high vibration amplitudes may indicate system malfunction or severe inflow conditions. The processing of raw signals to derived parameters can help to determine if it is motivated to bring the turbine to a de-rated mode of operation or to a complete stop state until the unit is further investigated and/or repaired.

In recent years nacelle vibration signals have become important also in active control systems, where the main target is to reduce loads through activation of blade pitch systems or by adding periodic components to the generator torque. In this case the signals are often filtered and processed within the control software, and accelerations are seldom communicated through the SCADA interface with enough resolution to be useful for any post-analysis.

Yet another system of a modern wind turbine where vibration measurements are essential is the *Condition Monitoring System* (CMS). Here mainly components of the drive train have sensors attached, but since the frequency ranges of interest normally are > 5 Hz , the focus on the frequencies around the tower resonance frequency might not be sufficient.

However, as discussed in the parallel report of LoadMonitor (Carlén, 2017), nacelle vibration signals are very useful for monitoring of tower and foundation loads , where the main idea is to derive approximate load signals without doing direct load measurements. It might therefore be attractive to look into the possibility to install an independent measurement system in order to facilitate more advanced analyses of the behavior of selected turbines in a wind farm of interest. Depending on the overall objectives of a turbine/site investigation, the acceptable complexity and cost for a corresponding measurement project can vary significantly. Here the existence of a robust low-cost measurement device, that can securely be installed by a service technician, will clearly increase the possibility to plan and complete such a mission.

2.3.1 Description of the developed instrument

For the present study it was therefore decided to try to identify key components for the design of such a system, and after comparisons of a number of units within the MEMS category, the choice fell on the SCA103T-D04 unit from MURATA. The SCA103T-D04 can be used for digital (serial) as well as analogue communication, which makes it very versatile. Since the main use of this sensor is to work as an inclinometer, it will work out all the way down to DC (0 Hz). The effective sensitivity in digital as well as in analogue mode is below 0.1 mg, which was found sufficient in the present context.

For the 7 month field test together with the Zephir lidar, a standard Campbell CR 1000 logger was used. The CR 1000 has a built in stabilized 5V power supply, and for the current setup (Figure 2-4) a network unit was attached in order to facilitate external communication through a 4G modem. Figure 2-5 shows how the vibration sensor is installed on the turbine.

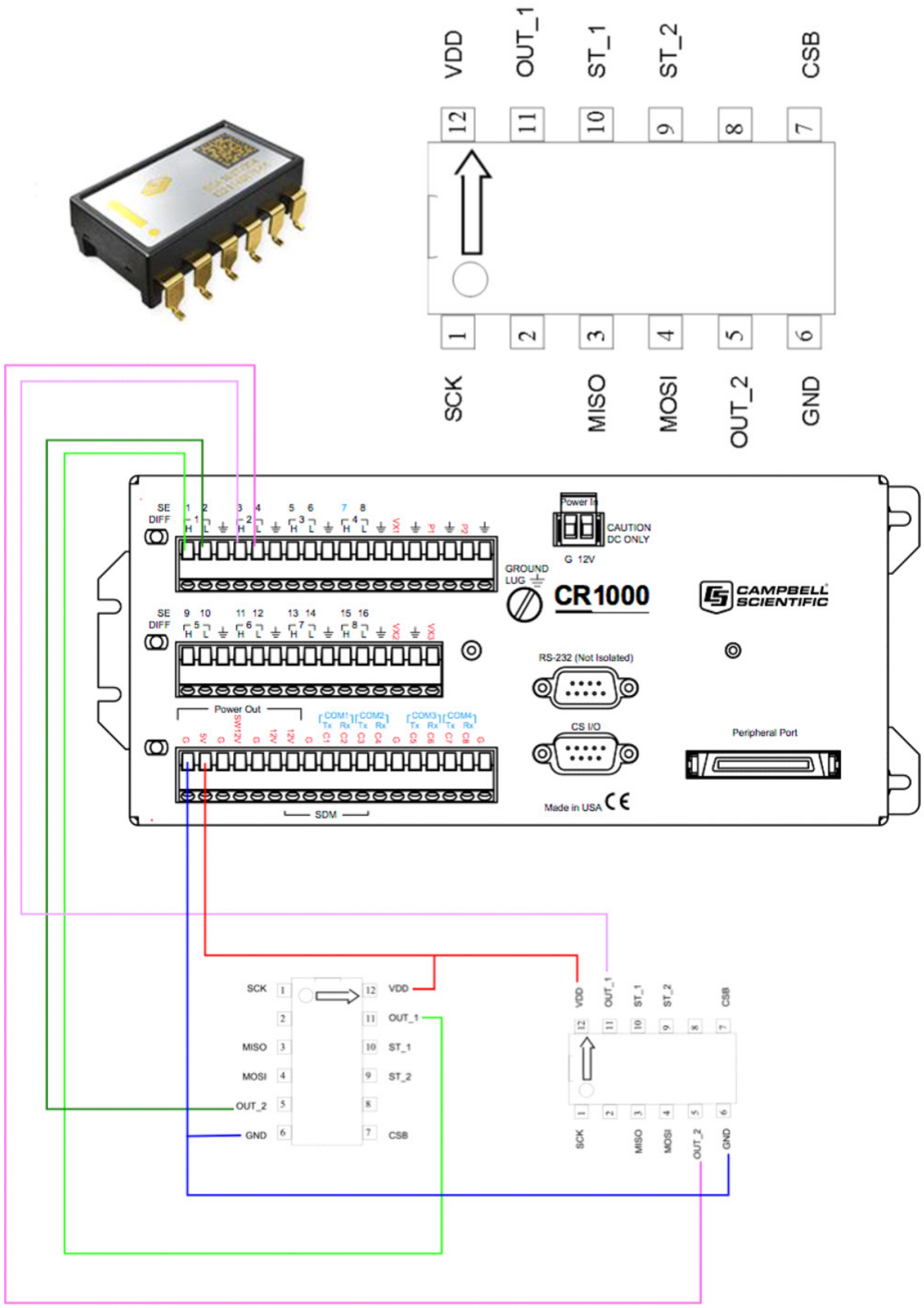

Figure 2-4: Two SCA103T-D04 connected for analogue communication with a standard Campbell CR1000 logger.

Figure 2-5: The cabinet containing the vibration sensors attached to a massive cast piece connecting the nacelle structure to the yaw bearing. The CR 1000 logger and the 4G modem was installed in sealed box towards the rear of the nacelle.

2.3.2 Description of data

Data was then downloaded at 03:00 every day, and every connection ended with a calibration of the CR 1000 internal clock to UTC time. During periods when the 4G service was unavailable (service provider experienced hardware failures), data was temporarily stored on a flash disk and then downloaded at a later occasion. Here a sampling frequency of 50 Hz was chosen, but in most cases a lower frequency may be sufficient. The lower limit is however determined by need for post-filtering dye to internal dynamics of the SCA103T-D04 around 11 Hz. For this reason the sensor is not suitable if frequencies higher than 4-5 Hz are of importance.

For the current setup only vibration amplitudes were measured since no detailed geometry information was available regarding the surface to which the sensor was attached, and subsequently a calibration of the zero inclination could not be performed. Figure 2-6 shows an example of raw and filtered lateral and longitudinal vibrations recorded by the instrument.

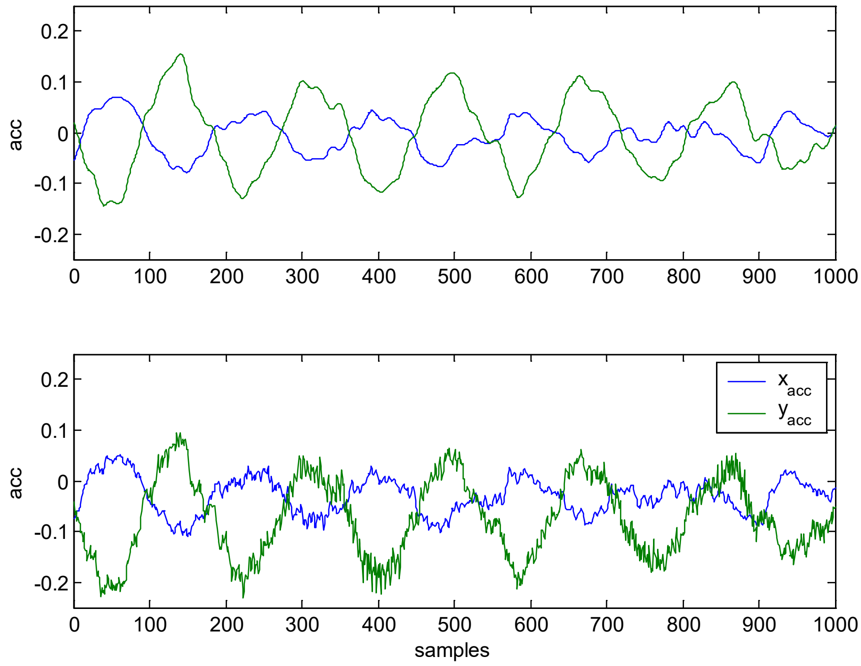

Figure 2-6: Examples of a short sequence (1000 samples / 20 s). Lateral and longitudinal nacelle vibrations, filtered and unfiltered respectively (3 order filter with cut-off at 5 Hz).

2.4 LES MODEL

2.4.1 LES and modifications to model forest and complex terrain

The Large-Eddy Simulations (LES) model was employed, where the large fluctuations of the wind flow are resolved in space and time (being the most important in the dynamic sense) while the effect of the small scales on the large scales is modelled. This is achieved by a decomposition of the Navier-Stokes equations into a filtered (or resolved) component and a residual (or subgrid scale, SGS) component. This way, the wind flow can be described by the LES equations in function of the boundary conditions and SGS model assigned to the problem. The modifications that are implemented to the model to represent the heterogeneous canopy, the rough ground as well as the varying topography that affect the flow above the forest are described below. Moreover, the ability to reproduce the wind field and the turbulence characteristics over the forest is further tested by comparing the quantities obtained from the lidar measurements to the values computed by a CFD simulation.

Computations were performed with the OpenFOAM platform, version 3.0.1. Based on the incompressible solver pisoFoam, available in the standard distribution of OpenFOAM, various modifications are implemented in order to represent the varying forest distribution into the LES. It is assumed that the forest acts as a porous surface exerting a drag on the flow. This is represented in the simulation with the introduction of a source term in the LES momentum equation

$$f_{D,i} = -C_D a \left|\overline{\mathbf{u}}\right| \overline{u}_i$$

where C_D is the forest drag coefficient, *a* is the frontal-area-density (assumed here equal to the PAD). This approach has been successfully used in wind computations over forest with LES, e.g. by Nebenführ (2015) and Boudreault (2015). The employed value of C_D =0.2 throughout the domain is taken from the latter. The effect of the subgrid scales is accounted for by using the SGS model of Yoshizawa (1986) where ν_{SGS} is estimated from the subgrid turbulence kinetic energy k_{SGS} which is in turn computed from a transport equation. This model is already available in OpenFOAM (kEqn), but modifications have to be performed to represent the dissipation of turbulence kinetic energy by the forest. This is done by adding the following term to the SGS equation:

$$\varepsilon_{\text{SGS}} = -\frac{8}{3} C_D a \left|\overline{\mathbf{u}}\right| k$$

A wall model is also used to account for the roughness of the ground, although it is expected that its influence on the wind flow will be much smaller in comparison to the forest. To this aim, the wall model implementation available in the OpenFOAM libraries of SOWFA (Churchfield, 2014) was employed. Hereby, the velocity deficit due to the interaction with the ground is introduced indirectly, by means of applying a surface stress. For this, the model of Schumann (1975) is used, where the non-zero components of the stress tensor at the surface are computed as a function of the friction velocity, which in turn is calculated from the logarithmic law with a local time-average for the horizontal velocity. Only the modules corresponding to the modelling of the surface stress are used from SOWFA, importing these from OpenFOAM 2.x into the version used for the simulations.

2.4.2 Numerical setup

The simulations are performed in a rectangular domain of dimensions $L_x \times L_y \times L_z$, = 16.48 km x 5.15 km x ~1.2 km (L_z varies due to the changing elevation of the terrain). WT04, where the lidar is mounted, is located at 12.875 km, in the middle of L_y. A top view of the bottom boundary of the computational domain (representing the elevation of the ground) is shown in Figure 2-8. The grid is produced with the mesh generator created by Gancarski & Chávez-Arroyo (2014), which adjusts the ground elevation to that of the varying terrain. The grid consists of 3 concentric zones in the horizontal plane: a farm zone at the interior (the most refined) which is then successively surrounded by a transition zone and a buffer zone. The two outermost regions can be described as rectangular edges. While the buffer zone has a width of 0.515 km for every edge around the domain, the transition zone regions are 1.03 km at the sides of the domain but different in the upstream (8.24 km) and downstream (1.545 km) regions of longitudinal direction, since it is desired to cover a large region ahead of the positions of measurement. The arrangement of the grid in the horizontal plane is uniform in the farm and buffer regions, while the cells stretch in the transition zone, changing the cell size from that of the farm to the one of the buffer zones. The terrain becomes flat at the buffer edges until, at the outermost boundary (with a width of 206 m), the elevation is uniform with a value of 155.57 m. The horizontal cell resolution is 10 m for the farm and 50 m in the buffer regions. The height of the first cell is ~2 m while the size increases vertically with a growing rate of ~1.04. These values are approximate due to the requirements of orthogonality in the direction of cell extrusion at the ground, while adjusting the cell heights to achieve a uniform elevation towards the top of the domain. In this way, the mesh is composed by a total of 29.55 x 10^6 cells.

The longitudinal axis of the domain is aligned with the wind direction for each case, so the inlet is perpendicular to the inflow. All lateral boundaries are set to periodic boundary conditions. Hence, the inlet flow is recycled from the outlet. The flow is driven by a uniform pressure gradient, following the procedure described by Bechmann (2006), which also comprises the introduction of Coriolis forcing (assuming a latitude of 58 degrees). In this manner, the pressure gradient is calculated for the desired geostrophic wind (10.5 m/s), which is set as to yield the desired wind velocity. The complete height of ABL is simulated to avoid the parametrization of the components of the shear stress, as they become negligible above approximately 1 km. The ground surface is set to a wall with a uniform roughness of z_0=0.03 m, while the PAD for the cells covering the tree area is extracted (by linear interpolation) from the file produced from the Airborne Laser Scans (ALS). While the real tree distribution is employed for the farm and transition regions of the grid, a constant PAD of 0.16 is employed at the buffer edges, extending along 4 cells in the vertical direction (equivalent to the average height of the trees in the simulation). The PISO algorithm is employed for the solution of the pressure-velocity equations. A backward interpolation scheme is applied in the solution of the transient term and central differencing for the remaining terms.

Simulations are run during about 120×10^3 s to develop the flow and achieve convergence of second-order statistics. Results are obtained during a subsequent computation lasting 20×10^3 s with Δt = 0.24 s, yielding a maximum Courant-Friedrichs-Lewy number of 0.67 over the whole domain. For the comparison with the lidar measurements, data is gathered by recording time-series of the velocity vector at every Δt and at the same locations as with the laser scan. In addition, averaged values of the velocity field, Reynolds stresses and subgrid TKE are computed at the location of the WT04 as well as 100 m and 200 m upstream from it.

2.4.3 Setting up the model at the site

In order to obtain input to the drag modelling of the forest Airborne Laser Scans (ALS) were downloaded from the data base of Lantmäteriet. The ALS data consists of high resolution backscatter data from an airborne lidar and carries information on the 3D coordinate of the backscatter point and the reflected intensity.

The points where mapped in a 10x10 m grid and the ground height was calculated as the median altitude of the returns in each 10x10 m gridbox, identified as ground returns by the data provider. Plant Area Densities, PAD, were calculated using the method of Boudreault et al. (2015), but with a weight of each data point corresponding to the fraction of return intensity out of the total return intensity of that particular beam. In that way it was possible to take into account the higher order return points of the beam (not just the first return).

The data set thus consisted of ground height and PAD with a vertical resolution of 1 m in a horizontal grid of 10x10 m. An example of a cut out of the region can be seen in Figure 2-7, where the forest height is shown and the sector chosen from model comparison is highlighted in colour. Likewise, Figure 2-9 to Figure 2-12 show the PAD distribution at different heights that is set in the LES simulation. These images will permit to establish a visual correspondence with the variation of TKE and the mean velocity distribution shown in the results.

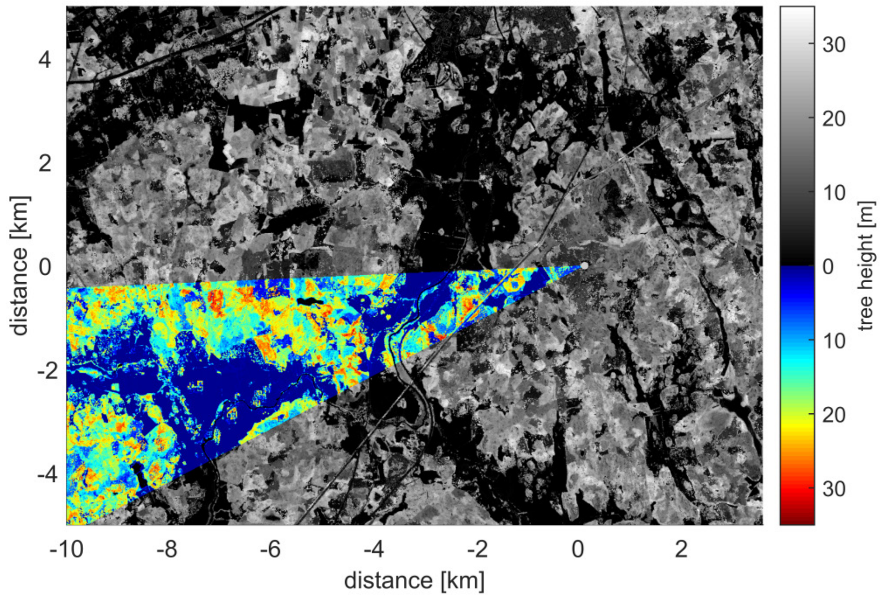

Figure 2-7: The tree height as derived from t[JL1]he Airborne Laser Scans. The wake-free sector chosen for model comparison is highlighted in coloring. The wind turbine equppied with the Zephir lidar is shown as a white filled circle.

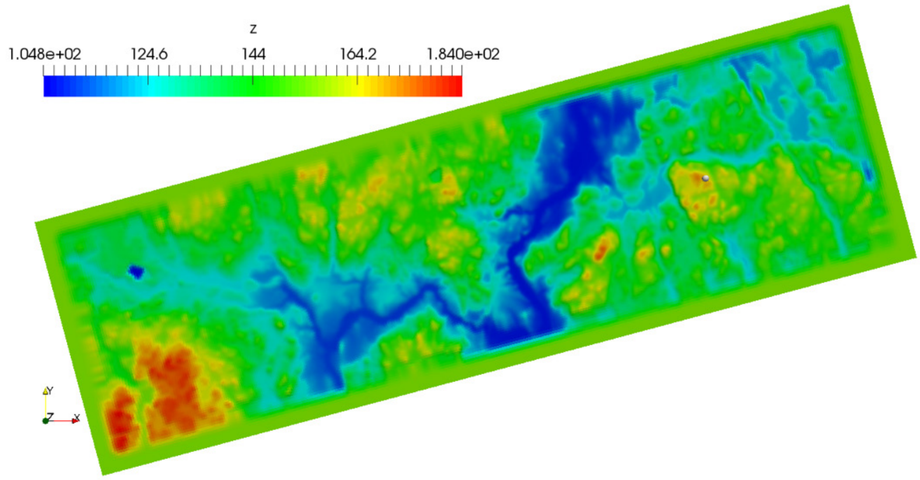

Figure 2-8: Terrain elevation in bottom surface of the computational domain. The small white circle on the right side represents the location of WT04, where the lidar is mounted.

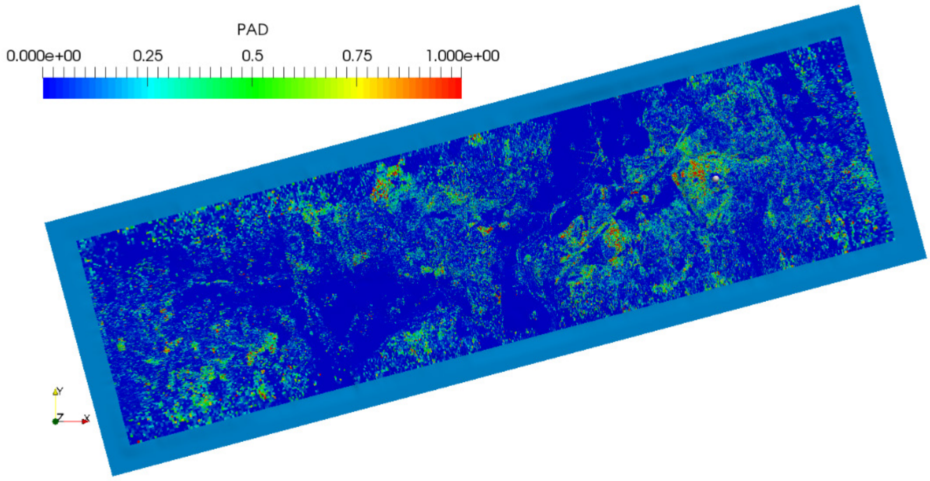

Figure 2-9: Plant area density distribution at 1 m from the ground.

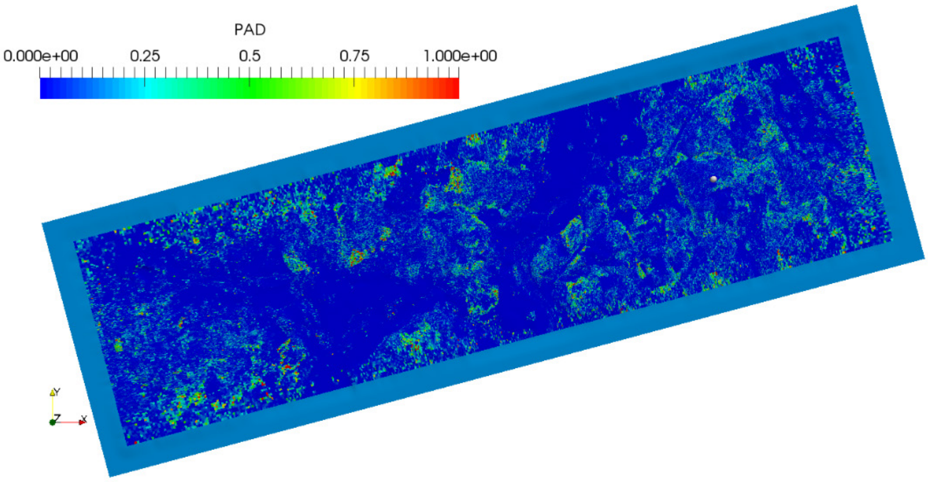

Figure 2-10: Plant area density distribution at 5 m from the ground.

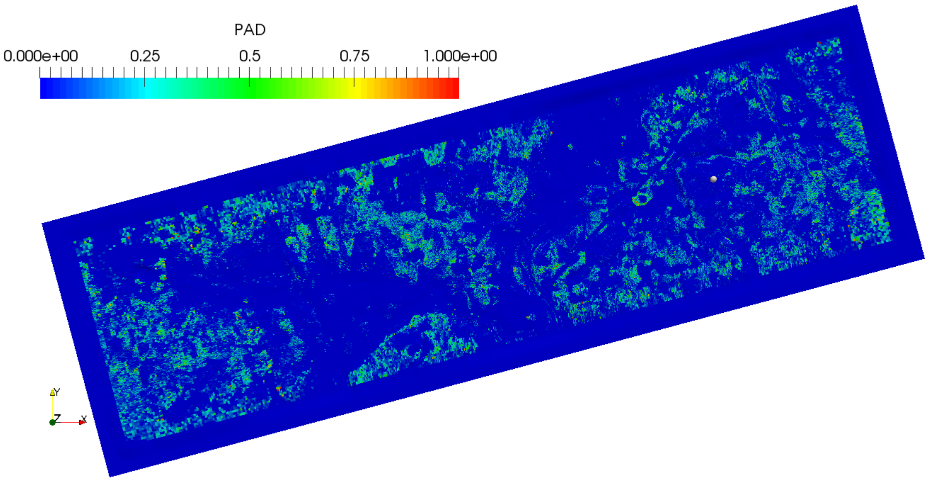

Figure 2-11: Plant area density distribution at 15 m from the ground

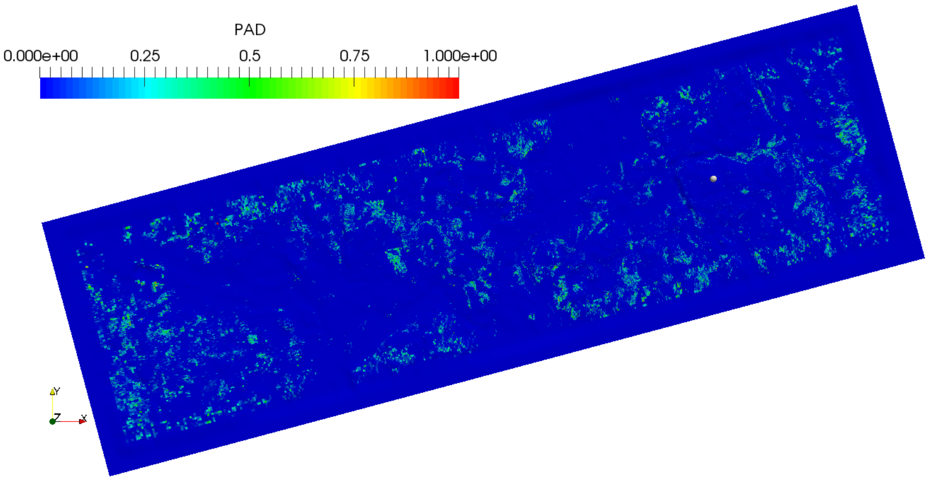

Figure 2-12: Plant area density distribution at 20 m from the ground

2.5 KVT MESO

At an early stage of the project it was realized that a measure of the atmospheric stability would add value to the other data sources of the project. Kjeller Vindteknikk has therefore carried out mesoscale numerical model simulations for the period of interest and over the region of the wind farm analyzed.

2.5.1 The WRF simulations

The Weather Research and Forecast (WRF) model has been used. WRF is a state-of-the-art meso-scale numerical weather prediction system, aiming at both operational forecasting and atmospheric research needs. A description of the modelling system can be found at the home page http://www.wrf-model.org/. The model version used in this work is v3.5.0 described in Skamarock et al. (2008). Details about the modelling structure, numerical routines and physical packages available can be found in for example Klemp et al. (2000) and Michalakes et al. (2001).

The most important input data are geographical data and meteorological data. The geographical data is from National Oceanic and Atmospheric Administration (NOAA). The data includes topography, surface data, albedo and vegetation. These parameters have high influence for the wind speed in the layers close to the ground. The ERA-Interim reanalysis data with approximately 0.7 degree resolution, available from the European Centre for Medium-Range Weather Forecasts (ECMWF) with 6 hours interval, is used as boundary data for the model (i.e. Dee et al., 2011). Surface roughness and landuse have been updated from Landmäteriets GSD database in Sweden.

The model setup uses four nested domains with an inner grid with 0.5 km x 0.5 km horizontal resolution. The model is run with 51 layers in the vertical with nine layers in the lower 200 m. The simulation outputs hourly data for the complete grid but for a number of pre-defined points, profiles of essential variables are written to file on model time step basis (2 s intervals). The simulated period is 2015-09-01 to 2016-06-22.

2.5.2 Atmospheric stability classification

Data from the WRF model is used to derive the atmospheric stability. In this analysis we have assessed the atmospheric stability with the static stability (*ss*) over the vertical layer confined by the upper tip of the rotor plane and the surface (150 m and 2 m) as:

$$ss = \frac{\Delta\theta}{\Delta z} ,$$

where $\Delta\theta$ is the difference in potential temperature over the vertical layer Δz. The classification used for the static stability is shown in Table 2.4. The specific thresholds defining the static stabilities are chosen such that there is a reasonable diurnal development of the stability classifications (Figure 2-13).

Table 2.4. Classification of static stability.

	$\Delta\theta/\Delta z$ [K/100m]
Unstable	< -0.1
Near-Neutral	ϵ [-0.1 1.0[
Stable	ϵ [1.0 4.0[
Very stable	≥ 4

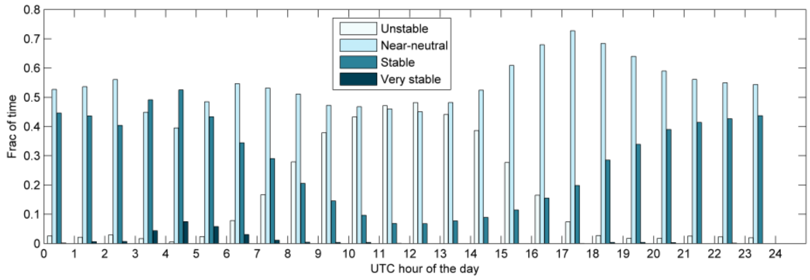

Figure 2-13: The diurnal distribution of the static stability classifications at the model grid-point closest to the turbine equipped with the Zephir Lidar.

It is difficult to assess the uncertainty in the simulated atmospheric stability since there is no possibilities to validate it at the site. There is an uncertainty related to the model data itself: stochastic uncertainties, for example related to the timing of weather systems, and potentially uncertainties related to systematic biases, for example in the surface energy budget of the model, which may result in erroneous diurnal evolution of the boundary layer etc.. Then there is uncertainties related to the stability classification itself (e.g. Holtslag et al., 2014), which was manifested in the LoadMonitor project where the classification was good enough to give clear stability signals in the production efficiency but was too coarse to precisely identify strict neutral episodes in the validation of the flow model.

2.6 DESCRIPTION OF SCADA AND WIND FARM CHARACHTERISTICS

The wind farm (WF) is located in southern Sweden where the winters typically are relatively short and mild. The terrain is rather simple and covered with production forest of varying height. The WF is composed of 11 2.5 MW turbines with a hub height of 98.5 m. It has been operational since 2012. The minimum distance between neighboring turbines varies from 3.9 to 4.7 rotor diameters with an average of 4.1 rotor diameters. The average tree heights in the wind farm area are changing between 8 m to 12 m according to the database of Swedish Forest Agency[1].

[1] Forest height data from Skogsstyrelsen (Swedish Forest Agency) http://www.skogsstyrelsen.se/skogligagrunddata

The terrain variation surrounding the turbine on which the Zephir Lidar is installed as well as the lidar's range circles in Figure 2-14.

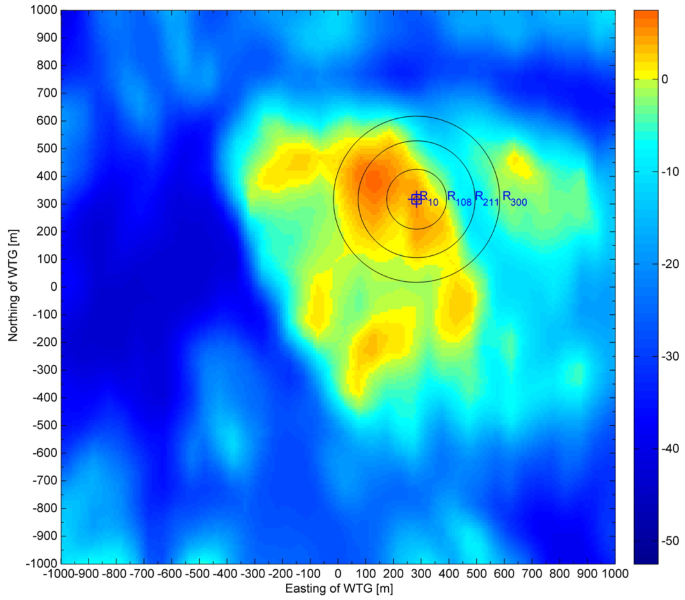

Figure 2-14: Terrain variation around the WT equipped with the Zephir lidar. The circles are showing the measurement ranges of the lidar used in the project.

SCADA data from the WF has been made available by the wind farm owner both as ten minute averages for all turbines and as 1 Hz data from the two turbines where the lidars have been located. Ten minute average data is available for the complete measurement campaign while 1 Hz data is available from 2016-01-11.

Many SCADA parameters were provided by the wind farm owner. The parameters that are included in the analysis are shown in Table 2.5 and introduced in the section where they are used.

Table 2.5. The SCADA parameters that have been available in the project.

Description	Unit
Turbine state	[-]
Alarm code	[-]
Power	[kW]
Nacelle position	[º]
Wind speed	[m/s]

There are other important input parameters that come from the chosen turbine and the WF.

- Rotor diameter and hub height of the wind turbine
- Turbine base elevation

- Power curve and its respective air density information to be used as reference in power curve analysis
- Rated, cut-in and cut-out wind speeds and rated power
- Digital terrain elevation map in the surrounding of the turbine
- Obstacles and neighbour turbines in the surrounding of the turbine (coordinates or relative position with overall dimensions)

2.6.1 Turbine offset and wake free sectors

The parameter "nacelle position" is found to deviate significantly between the turbines. It is also very different from the wind direction found in the KVT Meso data-set. It is beneficial to have information about the wind direction from the turbines instead of using the wind direction from the KVT Meso data-set. The timing of weather events can make the wind direction from KVT Meso to deviate significantly when looking at shorter time periods as is the case in several of the analyses in this project.

To identify wake-free and wake-contaminated sectors we have combined the SCADA parameter "nacelle position" and the ZDM "yaw misalignment" parameter and turbulence intensity (TI) on 10 minute basis. The upper panel in Figure 2-15 shows the nacelle position versus the yaw misalignment. When the ZDM scanning circle partially hits the wake from a neighbouring turbine it will interpret the signal as a yaw misalignment. An analysis of the yaw misalignment dependence on the nacelle position is therefore useful to identify the sectors with wake presence. Gray-shaded areas in Figure 2-15 indicate the sectors that have been identified to be in the wake of neighbouring WTs. All episodes when the WT's nacelle position is in the sectors with white background are assumed to correspond to wake-free conditions. Increased levels of TI are also seen in the sectors associated with wakes, although the scatter of the data is larger (lower panel of Figure 2-15). The ZDM also measures and quantifies the wind flow complexity by comparing the measured line of sight velocities (LOS) around the lidar's circular scan to a best-fit wind model. This wind flow complexity metric can also be used to identify turbine wakes or complex windflows caused by obstacles etc.

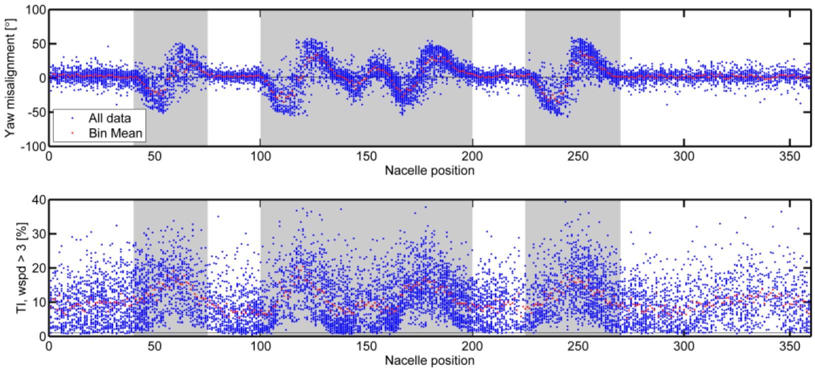

Figure 2-15: SCADA nacelle position versus Zephir Yaw misalignment (upper panel) and Zephir turbulence intensity (lower panel), based on 10 minute statistics. Grey markings indicate sectors that are contaminated by wakes. White background indicates sectors that are assumed not to be disturbed by wakes.

2.6.2 Filtering, identifying full-performance

The SCADA data can be filtered in various ways depending on how the data is going to be used. This section provides a general description of how data is filtered and may not be completely applicable for all aspects of the report.

It is essential that erroneous data is removed from the data set so that the results are not affected. If data is removed only for specific wind situations (high/low) any statistics derived from the data set is not likely to represent the true values for the period. Alarms related to high/low wind speeds may result in such bias. Icing might also cause such effects depending on during which weather situations icing occurs. This will be site dependent. Production is considered as partial- or non-performing when any of the following apply:

- Periods of curtailment.
- Periods identified as influenced by icing.
- An operating state that indicates that the WT is in non-normal operation. Through an analysis, an interval of operating states were identified to clearly be associated with full-performance, the remaining operating states were treated as partial- or non-performing and filtered out. This filtering is considered to be somewhat conservative. The time step after a flagged episode is also filtered out.
- Periods when neither of the above applies and the nacelle wind speed is well above cut-in wind speed but production is negligible.

In addition there are gaps in the SCADA data (missing data). The filtering is done on the 10-min SCADA data and the filtering flags and their time stamps are then transferred to the 1 Hz SCADA data.

3 Ambient conditions and wind turbine performance

3.1 DESKTOP STUDY - PERFORMANCE ASSESSMENT OF WIND TURBINES

The current state of the art in assessment of wind turbines performance has been focusing on developing new methods to assess the power curves with additional inputs available from the inflow wind conditions. As discussed in previous Elforsk research project ProdOptimize (Turkyilmaz & Undheim, 2016) many parallel work has been going on in the field of wind turbine performance assessment. The most known working platforms are such as the Power Curve Working Group (PCWG-1, 2016), the Technical Committee (TC) 88 of IEC (IEC TC 88, 2016) and IEA Wind (IEA Wind Task 32, 2016), which all are formed by wind industry and academics institutions.

PCWG: In assessment of real world power curves PCWG has contributed to the following outcomes on how turbine performance shall be assessed in the future (PCWG-2, 2016).

- Consensus on validation and development of new methods in power performance assessment: Rotor equivalent wind speed (REWS) and turbulence normalization (correction)
- Distinguish real world wind conditions by standard (inner range where performance shall be 100 % on average) and non-standard (outer range where performance shall be less than 100 %) atmospheric conditions by the help of power deviation matrix with turbulence intensity and wind shear (or rotor wind speed ratio) and/or wind speed
- Data and intelligence sharing with the use of results from tens of power performance tests
- Development of open source benchmarking exercises
- Development of open source power curve analysis tool
- Collaborate with IEC technical committee groups i.e. to complement the committee's standard documents preparation work, primarily with IEC 61400-12 in power performance measurements and secondarily IEC 61400-15 in assessment of site specific wind conditions (PCWG-3, 2016).

IEC: The IEC standard 61400-12-1 (IEC 61400-12-1, 2005) was recently updated with newly introduced methods. Below are some of the newly introduced parts in the new version of the standard (IEC 61400-12-1 Ed.2, 2017), relevant to PCWG's works listed:

- Definition of REWS in addition to the traditional hub height wind speed
- Inclusion of remote sensing devices (RSD) as alternative to met masts (requires validation with met mast measurements and has some limitations when terrain type is complex.)
- Data normalization methods:
    - × Wind shear correction when REWS measurements are available
    - × Wind Veer correction
    - × Turbulence correction
- Inclusion of wind shear in site calibration procedure

IEA: The sub task III of IEA Wind Task 32 "Wind Lidar Systems for Wind Energy Deployment" Phase 1 has contributed to valuable results on use of lidars for turbine performance evaluation namely "turbine assessment" with focus on power curves and loads. A three year extension to previous work, Phase 2, has been proposed in 2015 September (IEA Wind Task 32, 2015) with below listed topics which are connected to turbine assessment:

- site assessment
- power performance
- loads and control
- complex flow

In connection to IEA Wind Task 32 works a 4-year long research project named UNITTE (Unified Turbine Testing), with DTU Wind Energy as project coordinator, started in 2014 funded by Danish Council for Strategic Research (UniTTe, 2016). UNITTE aims for developing new methods for power curve and load assessment of wind turbines. UNITTE's work packages involve the following:

- Modeling of inflow wind conditions in flat and complex terrains
- Calibration of profiling nacelle lidars
- Full scale measurement campaigns: 5 measurement campaigns in flat and complex terrains
- Power curve measurements with nacelle lidar verification in flat and complex terrains
- Load assessment for reduction of load uncertainties with use of nacelle lidar

3.1.1 Wind conditions influencing performance: wind shear and turbulence

The previous sensitivity analyses of turbine performance to wind conditions have shown that scatter in power production is significant. Lundquist (Lundquist, 2010) presented that as result of atmospheric stability, the wind shear and the turbulence effects can cause the power output to vary by as much as 20 %.

As shown by Rareshide et al. (Rareshide, Tindal, Johnson, Graves, & Simpson, 2009) a theoretical wind shear influence on power output was analyzed using Bladed simulations (DNV GL, 2016). Based on the assumption of a simple power law and a mean wind speed of 10 m/s at the hub height, normalized power output has been found to be varying by about 1% for the wind shear exponents from 0 to 0.5. This is a theoretical variation of power output. The analysis of the observed data was resulted different than what was found from the theoretical approach.

R. Wagner focused on the impact of wind shear on power production in her PhD Thesis more thoroughly (Wagner, 2010). A detailed version of the sensitivity analysis was performed by Wagner. Based on the HAWC2Aero simulations (Larsen, 2008), the shear dependence of power output with changing wind speeds at hub height was derived. In addition, the difference in kinetic energy flux was included within topic of the rotor equivalent wind speed valid for the whole rotor disc. Wagner concluded that use of rotor equivalent wind speed approach decreased the scatter in the power curve, therefore decreasing the uncertainties. It also provided less dependency on the wind shear than the standard power curve approach. Moreover, the theoretical power curve dependence on varying turbulence intensity was also studied by Wagner. For the lower wind speeds increased turbulence intensity resulted with higher power output while for the higher wind speeds close to rated wind speeds resulted with lower output when compared to 0 % turbulence intensity (laminar flow). Therefore the normalization of power curves with turbulence intensity provided better representativeness of power curve which would lead to better (Annual Energy Production) AEP estimation.

A study based on data from the Great Plains/Midwest in the US showed a significant scatter in the relationship between wind shear and turbulence, especially when diurnal patterns were investigated (Rareshide, Tindal, Johnson, Graves, & Simpson, 2009). Although the correlation could be site specific, the plot of wind shear and turbulence was found to be useful in comparing the wind conditions of the site with IEC predefined design wind conditions. Filtering was applied to the data based on exclusion of data for wind shear exponent higher than 0.20 and turbulence intensity higher than 12. About 27 % of the 10 min average data samples remained after filtering and it was concluded that more detailed approach was needed in order to understand real life performance of wind turbines by covering the non-standard conditions.

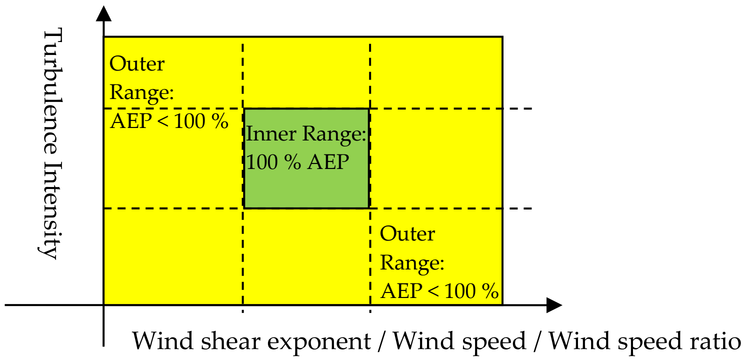

Figure 3-1: Inner/outer Range Matrix adapted from (Blodau, 2013).

In connection to the correlation plot of wind shear and turbulence, Blodau (Blodau, 2013) presented the power deviation matrix and its consequence on the AEP calculation. It was proposed that the AEP calculation should be made within an envelope to distinguish specific AEP calculations by standard wind conditions and for non-standard conditions as shown in Figure 3-1. This approach was used by PCWG as basis to build one of the main objectives as to investigate the impact of non-standard conditions on power production. Selection of boundary conditions of inner range was not fixed and it was recommended to be adjusted specific to chosen site’s wind characteristics.

A performance test was performed on a coastal site in Norway using ground based lidar data by Bardal et al. (Bardal, Sætran, & Wangsness, 2015). The results of sensitivity analysis of AEP difference (power curve derived AEP versus measured AEP) to turbulence intensity, wind shear and wind veer have been investigated with also taking into account the effect of use of rotor equivalent wind speed approach. The deviations were found up to 2 % especially for low wind shear and high turbulence conditions. The wind veer have been found to have smaller effect with about 0.5 % deviation for the chosen site.

3.1.2 Wind conditions influencing performance: inflow angle

The inflow angle of the wind upstream the rotor, either as yaw (horizontal) error/misalignment or tilt (flow inclination) angle (vertical), effects the power output due to the projected (skewed) and reduced rotor swept area that is perpendicular to the upstream wind flow.

Schlipf et al. presented the relation between the static misalignment (angle) with formula of normalized power output varied directly proportional to the cubed cosine of yaw angle (Schlipf, et al., 2011). With this approach it was shown that the static yaw error of 10 degrees could result with 4 % or more loss of power production.

In another publication by Højstrup (Højstrup, 2014) the relation between yaw error and loss of production was plotted with squared cosine of yaw error in order to better match low wind speed sites. The loss of production results obtained from this approach, also in the order of 4 %, were found to be agreeing with the simulations performed with Bladed for lower annual average wind speed sites.

3.1.3 Wind conditions influencing performance: forests

In the Elforsk Wind in Forest research project it was concluded that wind veer is significant at forested Swedish sites and the mean difference from lowest tip of rotor to highest tip can be more than 10 degrees (Bergström, et al., 2013).

Another study performed in UK by Derrick & Oram showed that tree felling around the turbines can change the wind conditions significantly (Derrick & Oram, 2014). Reduced wind shear and also reduced turbulence especially for the lower half of the rotor swept area were observed from onsite lidar measurements at a wind farm site. It must be noted though these findings might not be applicable on a homogeneous Swedish forest.

3.1.4 Relationships between the wind conditions and loads on the wind turbines

The wind conditions of a site has a major importance when the loads a wind turbine will be subject to is estimated. A desktop study of common load assessment techniques and load monitoring of wind turbines is presented in Appendix A. In the parallel second report (Carlén, 2017) vibration measurement, SCADA data, load measurements and aerolastic simulations of the Ryningsnäs wind farm are combined to find relationships between the vibrations and loads.

3.2 COMBINED ANALYSIS OF WIND CONDITIONS, VIBRATIONS AND SCADA DATA

Relationships between the vibrations and the ambient meteorological conditions are studied. The ambient conditions studied here are wind speed, wind shear, turbulence intensity, wind veer, horizontal inflow angle and the temperature in the form of atmospheric stability. No on-site measurements of atmospheric stability are made and the KVT Meso data set is used to derive the stability. KVT Meso and the stability are described in section 0. The data in the analysis are grouped according to three stability classes: unstable, near neutral and stable. It is found that the stability is having a significant influence on the relationships between the vibrations and the ambient conditions. This is not surprising as the atmospheric stability will influence the vertical profiles of the meteorological variables in the lower part of the atmosphere (the atmospheric boundary layer). There are many text books available giving thorough descriptions of the atmospheric boundary layer, see for example (Arya, 2001) and (Stull, 1988).

The wind direction will indirectly influence many of the studied variables since the terrain and ground cover is not homogenous at the site. Another thing that could influence the relationship between the vibrations and the meteorological variables is if the turbine is in the wake of another turbine or not; the wind in the wakes will be more turbulent than the wind outside the wakes. In order to make the interpretation of the results as easy as possible, only wake free conditions are considered. Read more about the identification of wakes in section 2.6.1.

Vibrations are measured in longitudinal (X) and lateral directions (Y). Relationships between both X and Y vibrations and the ambient conditions are shown in the following sections. Data classified as free from wakes and turbines in a full performance state[2] is in general used. It is clearly noted in the text associated with each figure if this is not the case. The ambient conditions are measured by the Zephir DM 200 m upstream of the rotor. Data from the period 2016-03-19 – 2016-06-21 is used in this section.

The measurements made in the project are from a wide temporal range (read more in Chapter 2). The majority of the comparisons are made in the time domain, but spectrums based on the vibration data is used to highlight the complexity of the relations between vibrations and the meteorology. The data sets are made homogenous by deriving all variables at a common time resolution. Different temporal resolutions are used. Which temporal resolution that is used is clearly stated in the subsequent sections.

The standard deviation of the vibrations is used as a measure of the vibration level in the different temporal resolutions investigated. The vibrations measured are accelerations in the X and Y directions. The accelerations are directly related to the displacement of the nacelle from its resting position. Hence, a high standard deviation indicates high acceleration and in turn also a large displacement of the nacelle.

3.2.1 Relationships between ambient conditions and vibrations

The results presented in this section are based on 10 minute statistics if not otherwise stated in the text. The vibration statistics used is the standard deviation in the 10 minute periods based on the 50 Hz data.

[2] A turbine is in full performance if it is working according to its technical specification and is not affected by curtailment, icing or any alarm code.

The standard deviation of vibrations over 10 minutes is a quite rough vibration estimate. The vibrations in 10 minute periods, expressed as spectrums, for a six hour period are shown in Figure 3-2. The ambient conditions during each 10 minute period are shown as text in the figure. Figure 3-2 shows that the wind speed measured by the ZDM lidar (<U>, ZDM) is around 4 m/s at the beginning of the six hour period (to the left in the plot) and between 9 and 10 m/s at the end of the six hour period (to the right in the plot). There are several frequencies contributing to the energy in the vibrations in each 10 minute period. The peak around 0.3 Hz is related to the first natural frequency of the tower, this is by far the dominating feature in the spectrums during low wind speed periods. Most of the peaks in the interval above the natural frequency of the tower and 1 Hz are related to the rotor blades passing the tower. The contributions in this interval are increasing as the wind speed is increasing due to the variable rotor speed of the turbine. The small peaks around 2.1 Hz is most likely related to the secondary natural frequency of the tower. An example of a low wind speed period, where the natural frequency of the tower is dominating is shown in Figure 3-3 and an example of a high wind speed period, where the blade passing induced vibrations are significant, is found in Figure 3-4.

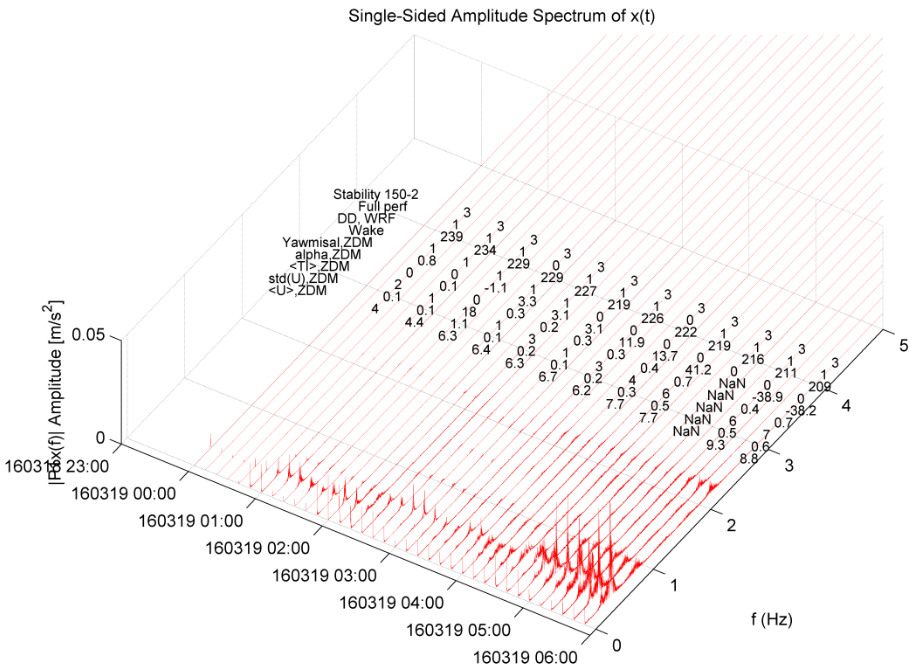

Figure 3-2: Spectrums based on the X-vibrations during 10 minute periods. The parameters shown as text in the top of the figure is <U>, ZDM: wind speed from the ZDM lidar [m/s], std(U), ZDM: standard deviation of the wind speed [m/s], <TI>, ZDM: Turbulence intensity [%], alpha, ZDM: wind shear exponent [-], Yawmisal, ZDM: yawmisalignment [°], Wake: 0 if the turbine is in a wake, 1 if not, DD WRF: modeled wind direction, FullPerf: 1 if the turbine is in full performance, 0 otherwise, Stability 150-2: Stability class according to Table 2.4.

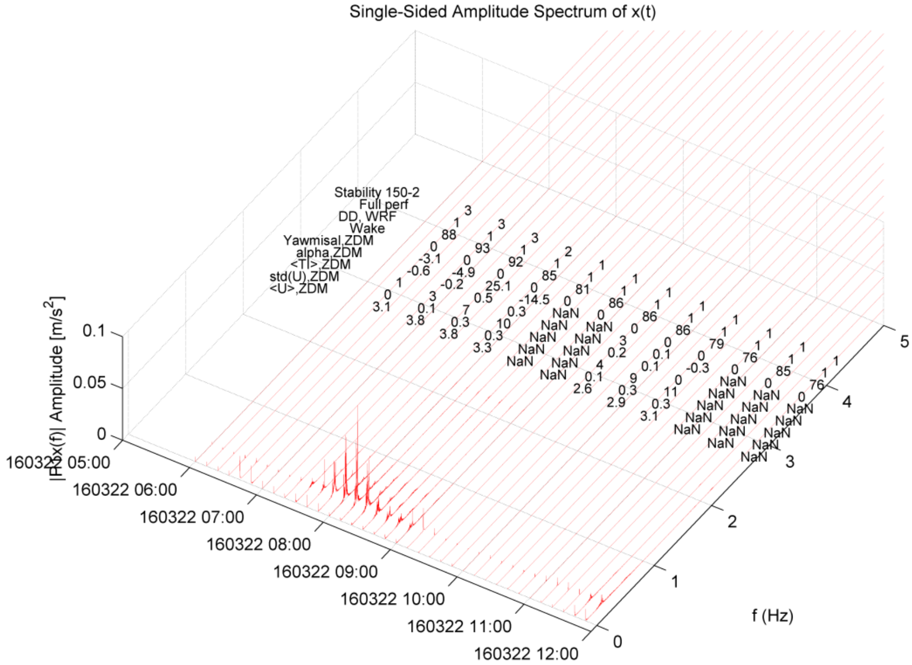

Figure 3-3: Spectrums based on the X-vibrations during 10 minute periods. The parameters shown as text in the top of the figure is <U>, ZDM: wind speed from the ZDM lidar [m/s], std(U), ZDM: standard deviation of the wind speed [m/s], <TI>, ZDM: Turbulence intensity [%], alpha, ZDM: wind shear exponent [-], Yawmisal, ZDM: yawmisalignment [°], Wake: 0 if the turbine is in a wake, 1 if not, DD WRF: modeled wind direction, FullPerf: 1 if the turbine is in full performance, 0 otherwise, Stability 150-2: Stability class according to Table 2.4.

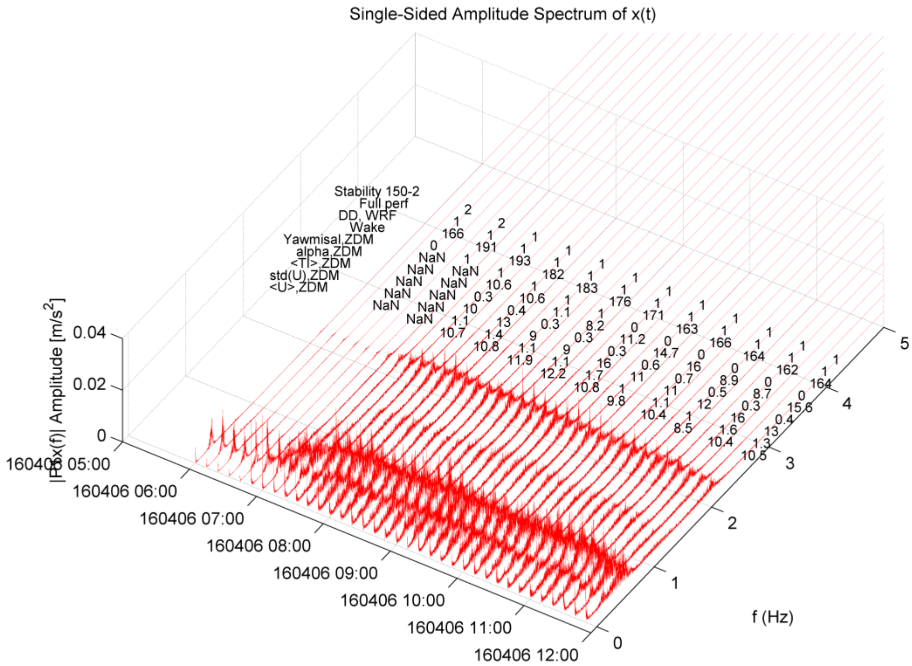

Figure 3-4: Spectrums based on the X-vibrations during 10 minute periods. The parameters shown as text in the top of the figure is <U>, ZDM: wind speed from the ZDM lidar [m/s], std(U), ZDM: standard deviation of the wind speed [m/s], <TI>, ZDM: Turbulence intensity [%], alpha, ZDM: wind shear exponent [-], Yawmisal, ZDM: yawmisalignment [°], Wake: 0 if the turbine is in a wake, 1 if not, DD WRF: modeled wind direction, FullPerf: 1 if the turbine is in full performance, 0 otherwise, Stability 150-2: Stability class according to Table 2.4.

Looking at plots like Figure 3-2 for a longer period in time it is clear that the appearance of the spectrums and the ambient conditions are complicated and not related in a simple way (not shown in the report). Note that periods when the turbine is in the wake of another turbine is included in Figure 3-2, Figure 3-3 and Figure 3-4. It is indicated if the spectrum is wake influenced in the figure with a 0. The value 1 indicates that the spectrum is wake free.

The above demonstrates that the standard deviation is a quite rough estimate of the vibration level and that signal processing (filtering) of the vibration data could isolate features that could be of interest. This is proposed as work for future research projects. Below is presented simple relationships between the vibrations and the ambient conditions. Only wake free and full performance occasions are included in the analysis.

In the following sections the results are presented for unstable, neutral and stable atmospheric stratifications. This categorization is based on mesoscale numerical model simulations and is further explained in Sect. 2.5.2.

Vibrations and wind speed

In Figure 3-5 it is seen that the level of longitudinal vibrations (here defined as the standard deviation over 10 minutes) is clearly increasing with increasing wind speed, measured by the Zephir DM lidar at a distance of 200 m in front of the rotor, for the unstable and near neutral cases while the increase is much smaller for the stable case. The smaller change of vibration level for the stable case is probably not related to the wind speed itself but to the characteristics of the wind flow during stable conditions; turbulence, wind shear and wind veer.

Figure 3-6 shows the lateral vibrations versus the wind speed. The pattern with increasing vibrations with increasing wind speed for unstable and near neutral conditions and less increase for stable conditions is similar to the longitudinal vibrations. But there is also one large difference, most clearly seen in the unstable and near neutral cases, and that is the presence of lateral vibrations that seem to be rather independent of wind speed. These are seen for standard deviations around 0.01 m/s^2. This makes the statistics in the lateral direction more difficult to interpret. It is found that this data mainly is from late May and June and for wind directions around north. This feature has not been studied further, it is proposed to continue to investigate this in future projects to establish if it is an anomaly in the measurements or if it is a real feature.

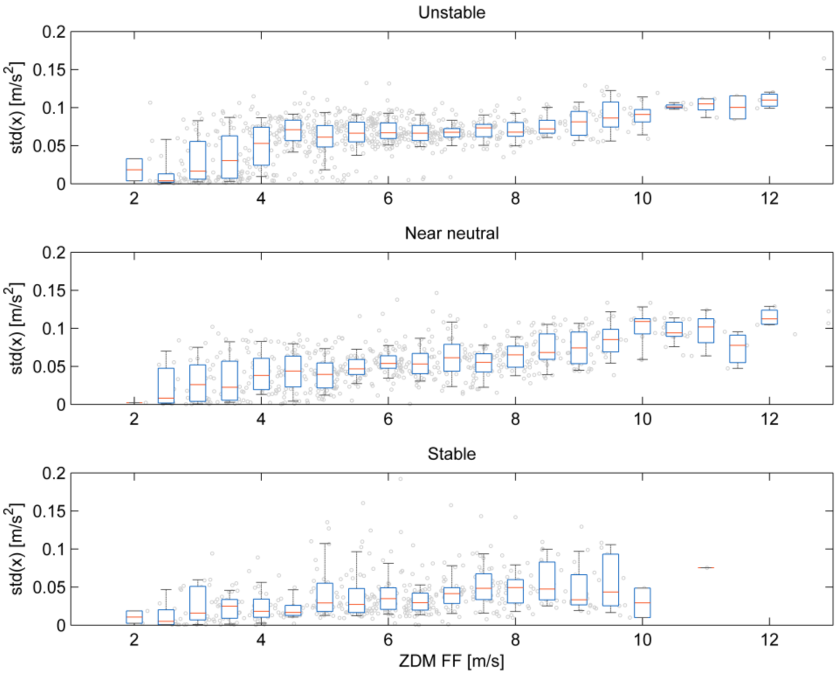

Figure 3-5: Wind speed at hub height from the Zephir vs. the standard deviation of the vibrations in the X-directon (longitudinal) in the case of unstable, near neutral and stable atmospheric stratification. The grey dots are the underlying data set. The boxes and whiskers show statistics over 0.5 m/s wide bins. The red line indicates the median value in each bin. The blue box shows the 25 and 75 percentiles. The whiskers span over an interval containing the points in the bin between 9 % and 91 %.

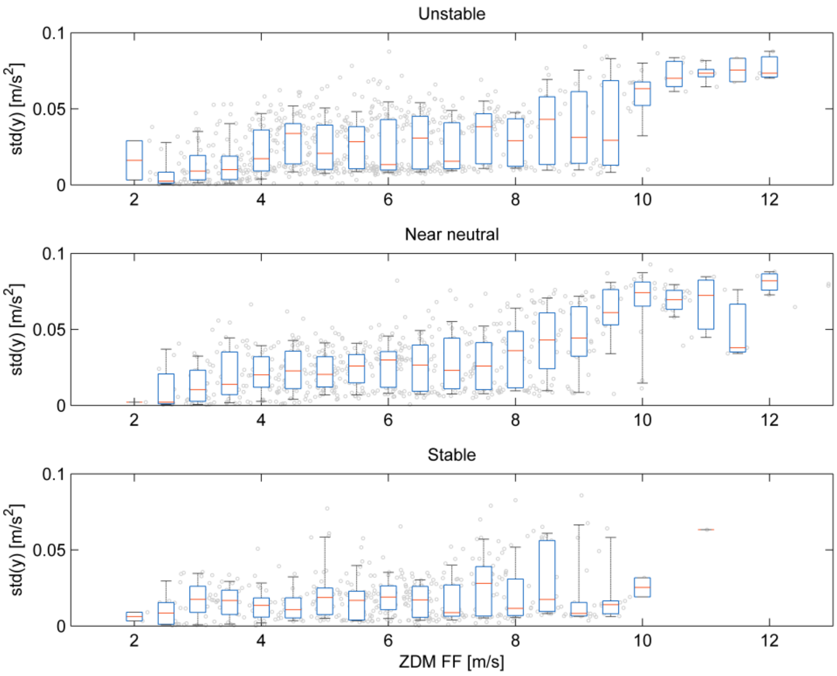

Figure 3-6: Wind speed at hub height from the Zephir vs. the standard deviation of the vibrations in the Y-directon (lateral), in the case of unstable, near neutral and stable atmospheric stratification. The boxes and whiskers show statistics over 0.5 m/s wide bins. The red line indicates the median value in each bin. The blue box shows the 25 and 75 percentiles. The whiskers span over an interval containing the points in the bin between 9 % and 91 %.

Vibrations and wind shear

Increased wind shear also means an increased level of longitudinal vibrations, Figure 3-7. This is the case for unstable, near neutral as well as for stable atmospheric conditions. It is somewhat intuitive to think that a large difference in wind speed over the rotor can induce more vibrations into the system compared to if the difference is small, especially as the wind profile is not linear. This pattern is also seen in the lateral vibrations, Figure 3-8. But as in the wind speed plots we see the more or less constant band of low vibration points affecting the statistics. Based on Figure 3-8 it seems like the low level vibrations are present for a wide range of wind shears.

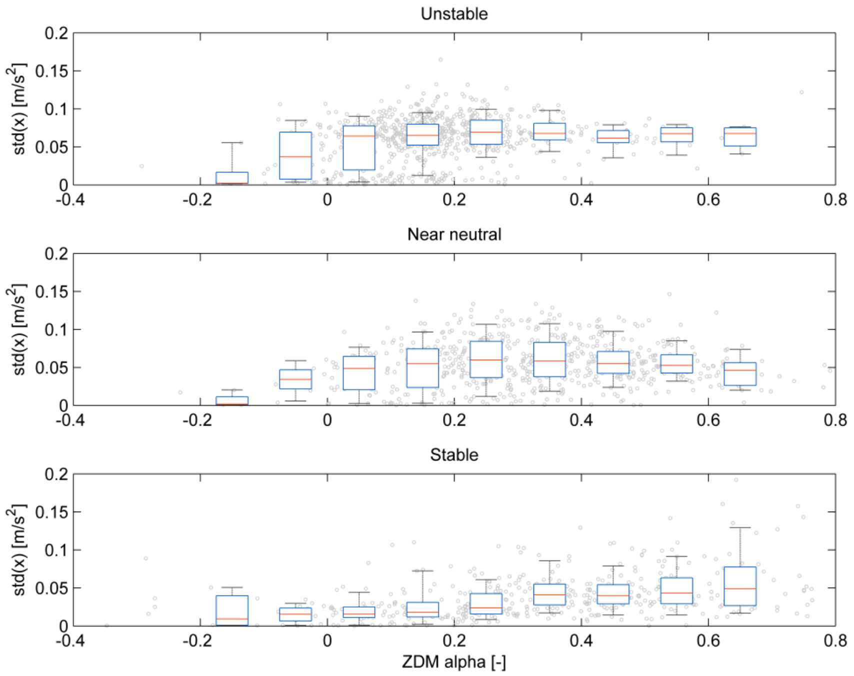

Figure 3-7: Wind shear exponent at hub height from the Zephir vs. the standard deviation of the vibrations in the X-directon (longitudinal) in the case of unstable, near neutral and stable atmospheric stratification. The grey dots are the underlying data set. The boxes and whiskers show statistics over 0.1 wide bins. The red line indicates the median value in each bin. The blue box shows the 25 and 75 percentiles. The whiskers span over an interval containing the points in the bin between 9 % and 91 %.

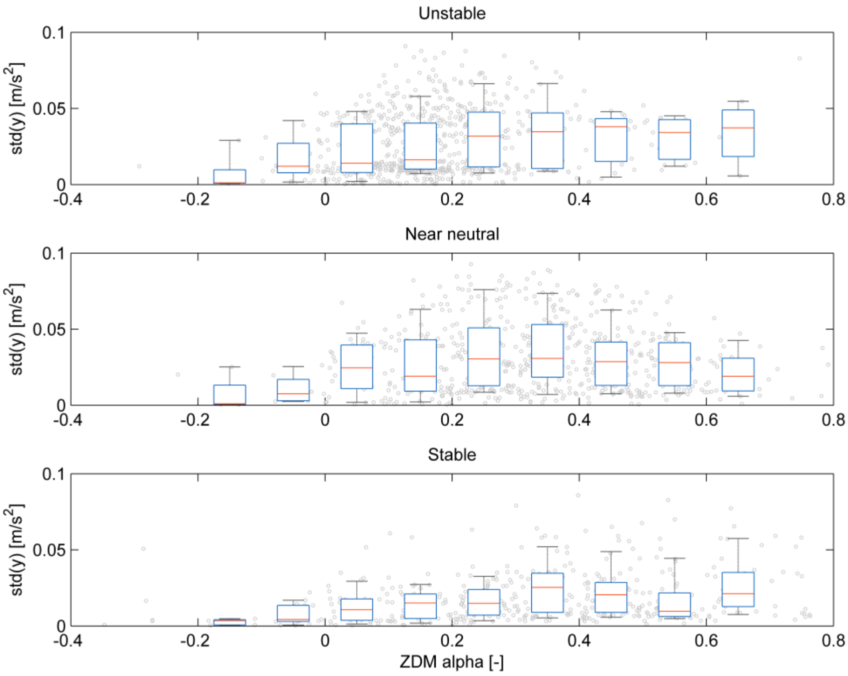

Figure 3-8: Wind shear exponent at hub height from the Zephir vs. the standard deviation of the vibrations in the Y-directon (lateral) in the case of unstable, near neutral and stable atmospheric stratification. The grey dots are the underlying data set. The boxes and whiskers show statistics over 0.1 wide bins. The red line indicates the median value in each bin. The blue box shows the 25 and 75 percentiles. The whiskers span over an interval containing the points in the bin between 9 % and 91 %.

Vibrations and turbulence intensity

In the longitudinal vibrations, Figure 3-9, the vibration level indicates a weak dependency on the turbulence intensity for the unstable case. The near neutral case shows a slight increase in vibration level with increased turbulence intensity. This can also be seen for stable conditions, but the amount of data in the higher bins is rather small. In the lateral vibrations, Figure 3-10, a similar pattern is seen. But also here the low level vibrations are found over a wide span of turbulence intensity making the patterns less visible.

The turbulence intensity is probably not the best characterization of the turbulence when the vibrations in the nacelle are studied. High frequency measurements with ultra sonic instruments could be used to derive the size of the turbulence elements during different atmospheric conditions. Such measurements are not available in the current project but are proposed as future work.

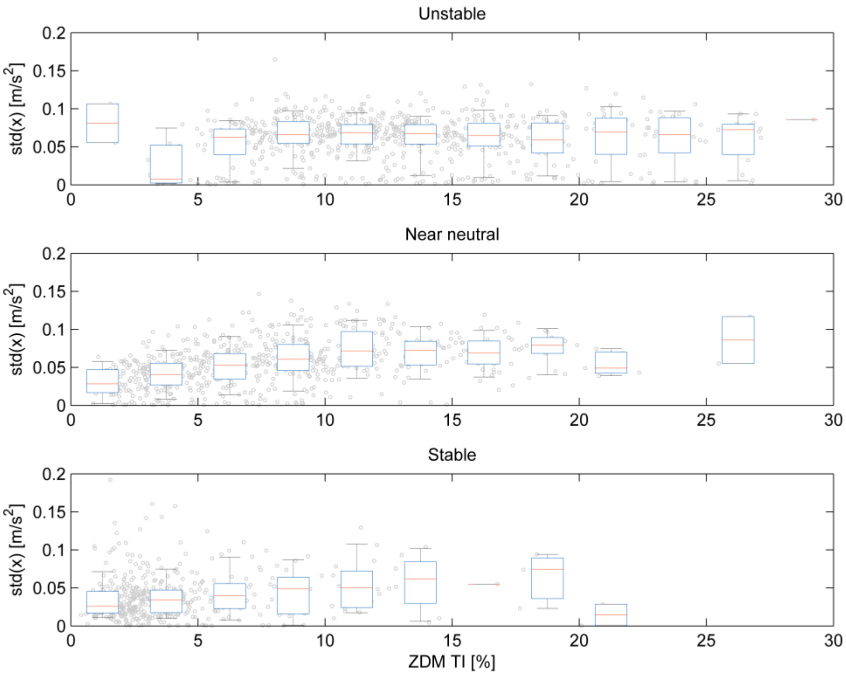

Figure 3-9: Turbulence intensity at hub height from the Zephir vs. the standard deviation of the vibrations in the X-directon (longitudinal) in the case of unstable, near neutral and stable atmospheric stratification. The grey dots are the underlying data set. The boxes and whiskers show statistics over 2.5 % wide bins. The red line indicates the median value in each bin. The blue box shows the 25 and 75 percentiles. The whiskers span over an interval containing the points in the bin between 9 % and 91 %.

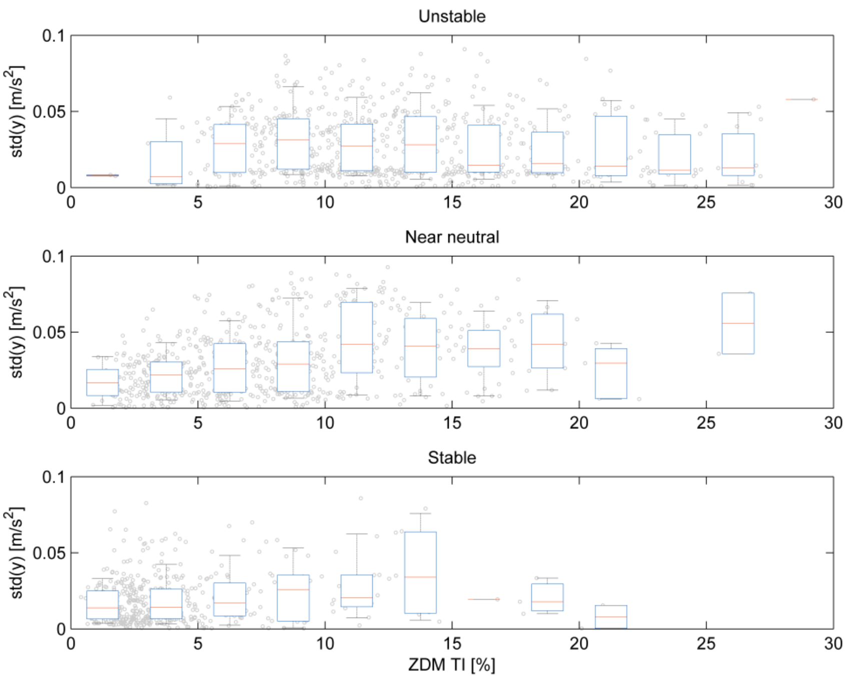

Figure 3-10: Turbulence intensity at hub height from the Zephir vs. the standard deviation of the vibrations in the Y-directon (lateral) in the case of unstable, near neutral and stable atmospheric stratification. The grey dots are the underlying data set. The boxes and whiskers show statistics over 2.5 % wide bins. The red line indicates the median value in each bin. The blue box shows the 25 and 75 percentiles. The whiskers span over an interval containing the points in the bin between 9 % and 91 %.

Vibrations and wind veer

The wind veer is derived from concurrent observations of yaw-misalignment from the Zephir DM at the measurement levels 57 m and 140 m above ground. The longitudinal vibration levels don't show any strong dependence on the wind veer, Figure 3-11. The same holds for the lateral vibrations, Figure 3-12, although the low level vibrations discussed above is present also for a wide range of wind veers, affecting the statistics. Note that the veer is close to symmetrical around 0° in the case of unstable and near neutral conditions while it is not during unstable conditions.

Intuitively, one could expect that an increased wind veer also would increase the vibrations in the nacelle due to imbalances in the rotor. This matter should be examined also in future measurement campaigns.

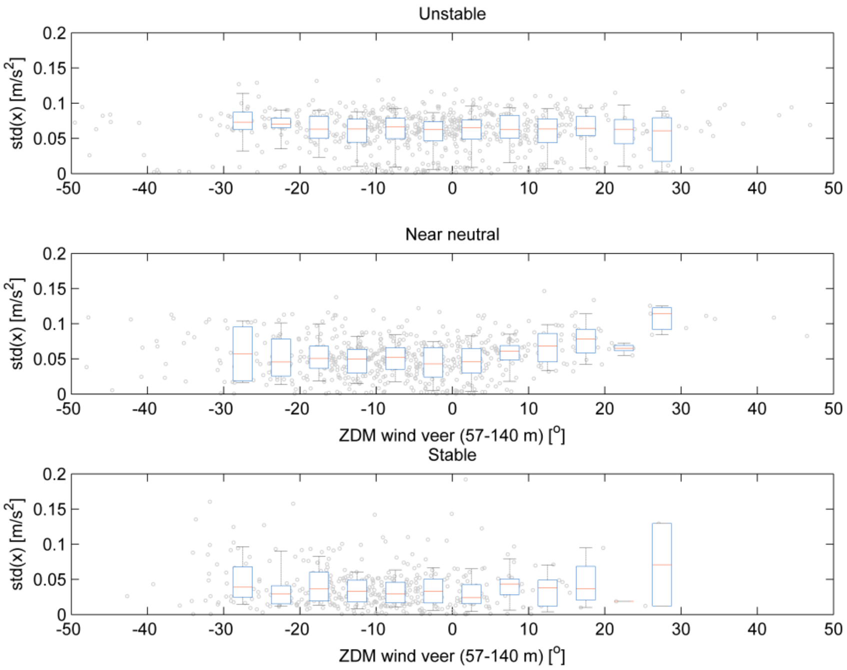

Figure 3-11: Wind veer between 57 m and 140 m from the Zephir vs. the standard deviation of the vibrations in the X-directon (longitudinal) in the case of unstable, near neutral and stable atmospheric stratification. The grey dots are the underlying data set. The boxes and whiskers show statistics over 5 ° wide bins. The red line indicates the median value in each bin. The blue box shows the 25 and 75 percentiles. The whiskers span over an interval containing the points in the bin between 9 % and 91 %.

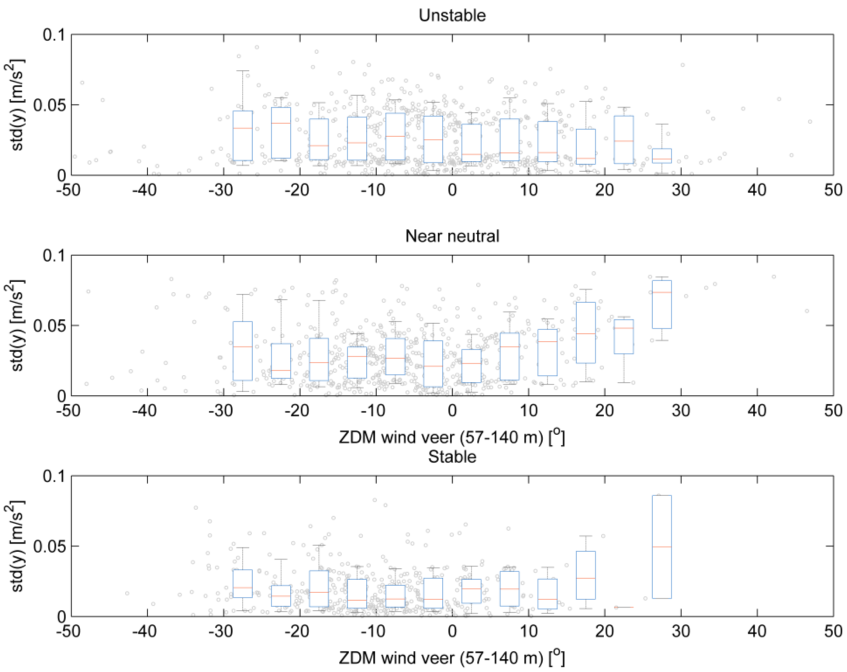

Figure 3-12: Wind veer between 57 m and 140 m from the Zephir vs. the standard deviation of the vibrations in the Y-directon (lateral) in the case of unstable, near neutral and stable atmospheric stratification. The grey dots are the underlying data set. The boxes and whiskers show statistics over 0.5 ° wide bins. The red line indicates the median value in each bin. The blue box shows the 25 and 75 percentiles. The whiskers span over an interval containing the points in the bin between 9 % and 91 %.

Vibrations and horizontal inflow angle

The yaw misalignment measured at hub height is used as the inflow angle of the wind towards the turbine. As for the wind veer, variations in the horizontal inflow angle does not seem to cause very large changes in the vibration levels either for the longitudinal, Figure 3-13, or the lateral, Figure 3-14 when the atmospheric stability is unstable or near neutral. During stable conditions there is an increase in vibration level with increased horizontal inflow angle. The low level lateral vibrations previously discussed are present for a rather wide range of inflow angles.

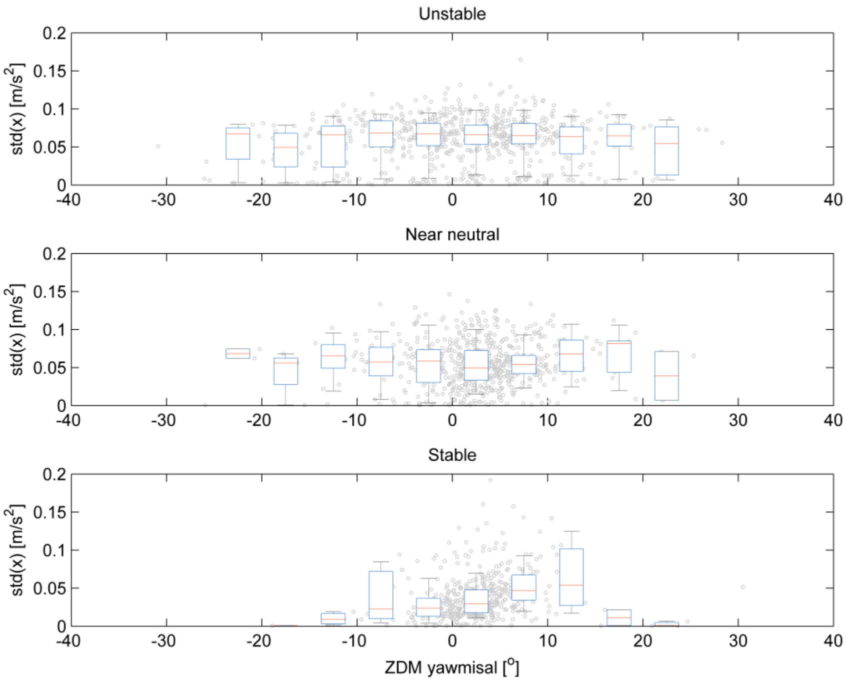

Figure 3-13: Horizontal inflow angle based on the yaw misalignment from the Zephir at hub height vs. the standard deviation of the vibrations in the X-directon (longitudinal) in the case of unstable, near neutral and stable atmospheric stratification. The grey dots are the underlying data set. The boxes and whiskers show statistics over 5 ° wide bins. The red line indicates the median value in each bin. The blue box shows the 25 and 75 percentiles. The whiskers span over an interval containing the points in the bin between 9 % and 91 %.

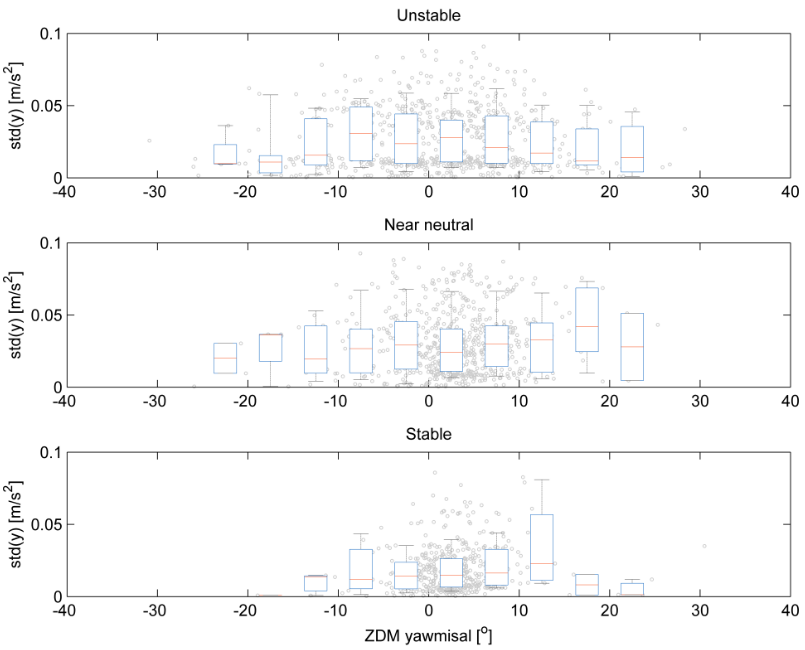

Figure 3-14: Horizontal inflow angle based on the yaw misalignment from the Zephir at hub height vs. the standard deviation of the vibrations in the Y-directon (lateral) in the case of unstable, near neutral and stable atmospheric stratification. The grey dots are the underlying data set. The boxes and whiskers show statistics over 5 ° wide bins. The red line indicates the median value in each bin. The blue box shows the 25 and 75 percentiles. The whiskers span over an interval containing the points in the bin between 9 % and 91 %.

3.2.2 Relationships between ambient conditions, vibrations and production efficiency

In this section we investigate whether vibration and environmental data can be related to the performance of the turbine. As was the case in 3.2.1, data from the period 2016-03-19 – 2016-06-21 is also used here, but to increase the amount of data, 1 minute rather than 10 minute statistics are used. With a shorter time averaging it becomes increasingly important to have the different data sources properly synchronized. During the period analyzed here, the Zephir measures the ambient conditions at a 200 m range (configuration 3, see section 2.2). This implies a time-difference in the sampling of the ambient conditions by the Lidar and by the SCADA system that is significant compared to the 1 minute averaging window. In addition, the sampling time-difference varies with the wind speed. In this analysis, when production efficiency is investigated, the wind speed is therefore based on the nacelle anemometer.

We define a relative production efficiency ($PE_{wi,vi}$) at a certain wind speed interval, *wi*, and a certain interval of a secondary variable *vi* as:

$$PE_{wi,vi} = \frac{\mathrm{P_{wi,vi}}}{\frac{1}{N}\sum_{vi=1}^{vi=N} P_{wi,vi}} \qquad \text{Eq. 1}$$

Where $P_{wi,vi}$ is the average measured production during the episodes when wind speed is confined to interval *wi* and when the secondary variable is confined to interval *vi*. The sum in the denominator of Eq. 1 therefore represent the average production at a given wind speed interval and $PE_{wi,vi}$ is interpreted as the deviation from the average production at the specific wind speed interval. A $PE_{wi,vi}$ smaller or larger than 100% indicates that the turbine is producing less or more than normal for that specific wind interval, respectively. The secondary variable can for example be vibrations, wind shear exponent, turbine misalignment etc.

If not explicitly stated otherwise all the following results are **based on wake-free conditions** and only on episodes when the turbine is considered to **be in full performance**[3].

Figure 3-15 shows the 2d-histogram of the nacelle wind speed and the longitudinal vibrations regardless of atmospheric stability as well as for unstable (convective), near-neutral and stable atmospheric conditions. The figure shows that more stable conditions are associated with a weaker signal in the vibrations (the higher densities are found in the lower part of the "cloud") and that there is a more evident relationship between wind level and vibrations in the unstable and near neutral case compared to the stable case, which was also seen in Figure 3-5.

[3] A turbine is in full performance if it is working according to its technical specification and is not affected by curtailment, icing or any alarm code.

Figure 3-15: Density scatter plots of wind speed from the nacelle anemometer and the 1-minute standard deviation of the longitudinal component of the vibrations. Right panel shows the 2D-histogram for all wake-free, full performance episodes, regardless of atmospheric stability. Lower panels show the same data but separated with regards to atmospheric stability. Colors indicate the fraction of the data in each wind-speed/vibration bin. Bins with less than five 1-min values are not plotted.

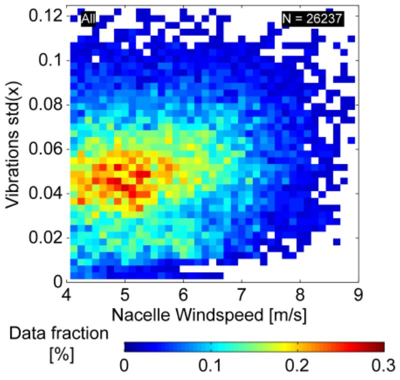

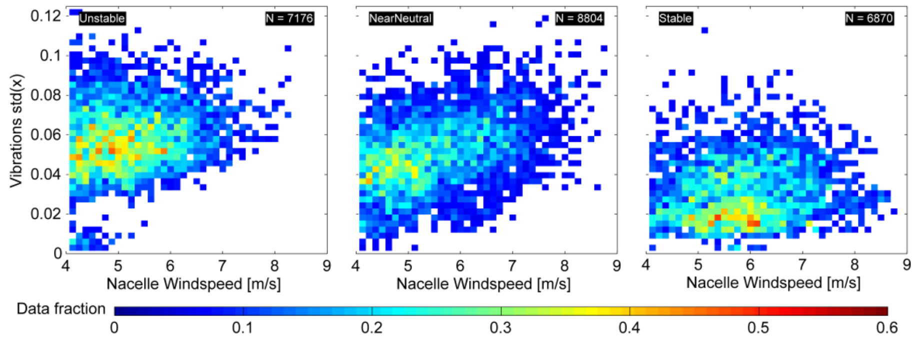

Figure 3-16: Relative production efficiency (PE) as a function of nacelle wind speed and the variability of the longitudinal vibrations. Right panel based on all wake-free, full performance episodes, regardless of atmospheric stability. Lower panels show the same data but de-constructed with regards to atmospheric stability.

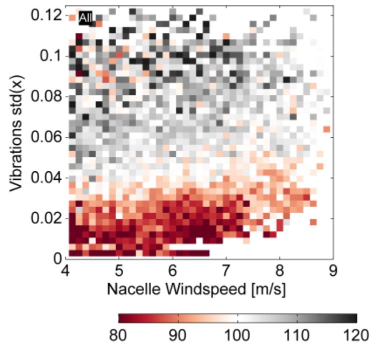

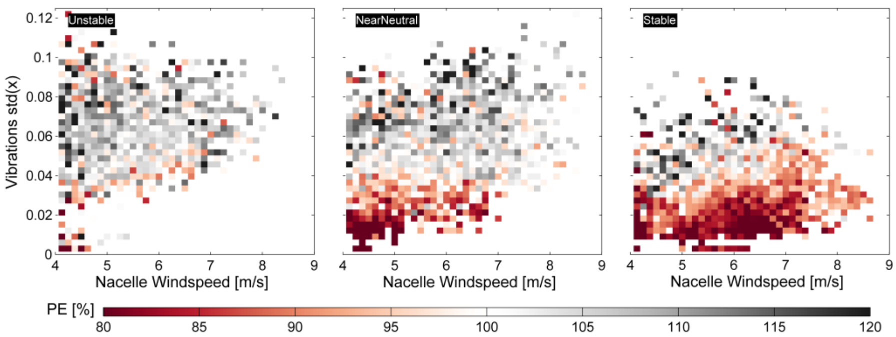

Figure 3-17: Relative production efficiency (PE) as a function of nacelle wind speed and the variability of the lateral vibrations. Right panel based on all wake-free, full performance episodes, regardless of atmospheric stability. Lower panels show the same data but de-constructed with regards to atmospheric stability.

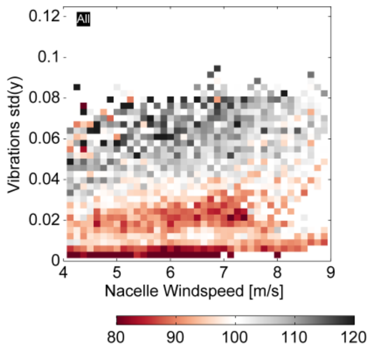

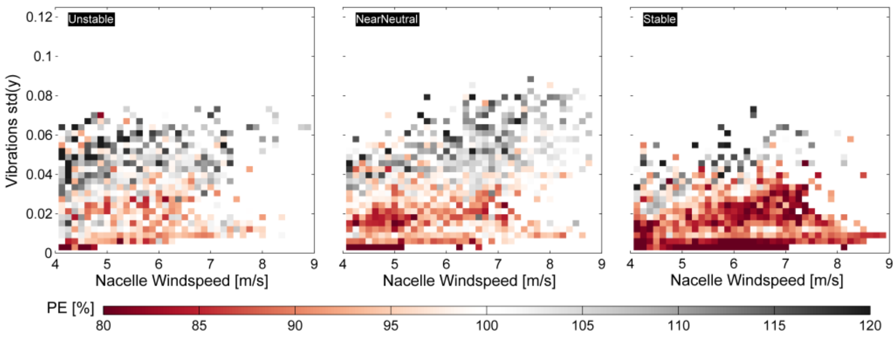

In Figure 3-16/Figure 3-17 the relative production efficiency (PE) is projected upon the distribution-cloud that is spanned up by the nacelle wind speed and the standard deviation of the longitudinal/lateral vibrations. The upper right panels show that smaller vibrations are associated with lower PE-values. If the data is grouped with respect to the atmospheric stability it becomes evident that a large part of the instances of low PE origins from episodes with stably stratified atmospheric conditions. On the other hand, convective (unstable) atmospheric condition is to a large extent associated with high PE-values.

With stably stratified atmospheric condition we for example expect lower turbulence levels and larger vertical wind shears compared to convective atmospheric conditions, two factors that are known to influence the production efficiency (e.g. Bardal et al., 2015 and Vanderwende and Lundquist, 2012). In the following figures we will investigate if, and how, characteristics of the ambient flow affect the production efficiency.

In Figure 3-18 the PE is projected upon the distribution-cloud that is spanned up by the nacelle wind speed and the vertical wind shear exponent (α, derived by the Zephir Lidar at a 200 m scanning range). The upper right panel shows the results if all data is considered, regardless of atmospheric stability. There is a weak signal of PE increasing with increasing wind shear exponent. This might be explained by the fact that, theoretically, for small (positive) wind shear exponents the nacelle wind speed will overestimate a rotor equivalent wind speed while for larger wind shear exponents the relation is the opposite. The critical value of α when the overestimation turns into an underestimation depend on wind speed and turbine dimensions (e.g. Bardal et al., 2015).

When the data is grouped with respect to the atmospheric stability (lower panel of Figure 3-18) it again comes evident that much of the episodes of lower production efficiency are connected to stably stratified flows. Only for the stable cases there is wind speed invariant relationship that higher α-values are associated with larger PE-values and vice versa. For the unstable cases there is no clear signal in the PE with respect to α and for the near-neutral cases there is an indication that larger α-values are associated with larger PE at higher wind speeds.

In Figure 3-19 the PE is instead projected on the distribution-cloud that is spanned up by the nacelle wind speed and the turbulence intensity (TI, here evaluated on a 1 minute basis based on the nacelle anemometer). For the all cases (upper right panel) we see a clear pattern that higher TI-levels are associated with higher PE. It is expected that turbulence will increase the power for wind speeds below the inflection point of the power curve. For the period analyzed wind speeds are hardly reaching inflection point wind speed. There is however an indication of weaker TI-dependence of the PE at the higher wind speeds.

When the data is grouped with respect to atmospheric stability (lower panel of Figure 3-19) it is clear that the static stability categories represent very different turbulent regimes (through the location of the distribution clouds). For all three stability classes PE increase with increased TI.

Figure 3-18: Relative production efficiency (PE) as a function of nacelle wind speed and the vertical wind shear exponent (α). Right panel based on all wake-free, full performance episodes, regardless of atmospheric stability. Lower panels show the same data but de-constructed with regards to atmospheric stability.

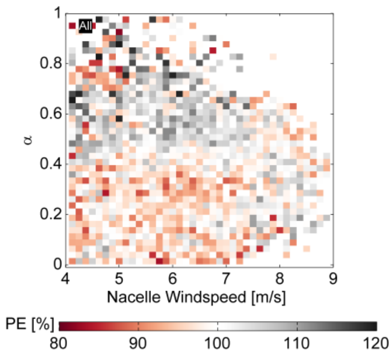

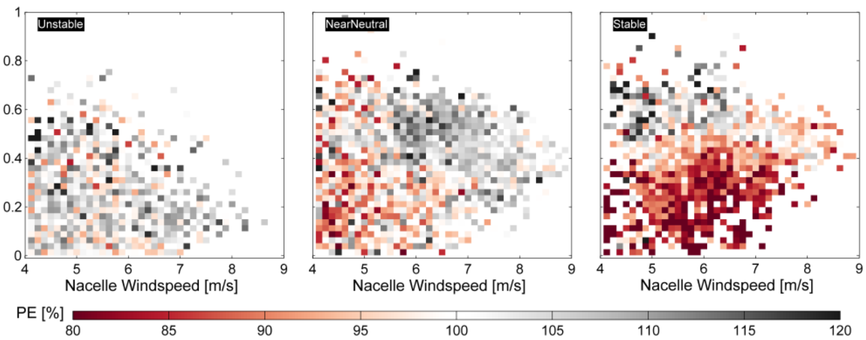

Figure 3-19: Relative production efficiency (PE) as a function of nacelle wind speed and the 1-minute turbulence intensity (TI). Right panel based on all wake-free, full performance episodes, regardless of atmospheric stability. Lower panels show the same data but de-constructed with regards to atmospheric stability.

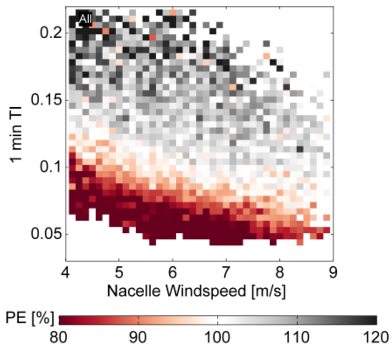

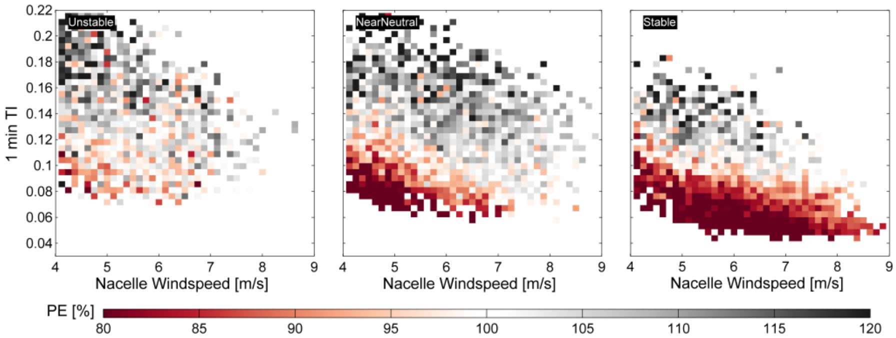

Figure 3-20 shows the PE projected on the distribution cloud that is spanned up by the nacelle wind speed and the yaw misalignment (as retrieved by the Zephir Lidar). The results when all data (regardless of stability) is considered can easily be misinterpreted (upper right panel). There is no reason to expect small values of yaw misalignment to be associated with low production efficiency as seen in the figure, instead other parameters are responsible for this results. If the data is grouped (lower panel Figure 3-20) we see very different distribution-clouds for the different stability cases. In the stable cases the variability of the yaw misalignment (illustrated by the cloud width in the y-direction) is considerably smaller compared to the unstable and near-neutral cases. The explanation for this is likely that the WT control system has an easier job with a more laminar flow, which results in smaller yaw misalignment with increasing atmospheric stability. As we have seen previously, stable atmospheric conditions are in general associated with low PE, which we primarily connect to lower turbulence levels compared to the unstable and neutral conditions (Figure 3-18 and Figure 3-19).

The variation of the wind direction with height, i.e. the wind veer, also influences the production efficiency but has not been addressed here. However, note that there is a considerable wind veer associated with the stable atmospheric episodes. On average the veer is about 10° from the lower to the upper tip of the rotor swept area for stable situations (Figure 3-11, based on 10 minute statistics).

Figure 3-20: Relative production efficiency (PE) as a function of nacelle wind speed and the yaw misalignment. Right panel based on all wake-free, full performance episodes, regardless of atmospheric stability. Lower panels show the same data but de-constructed with regards to atmospheric stability.

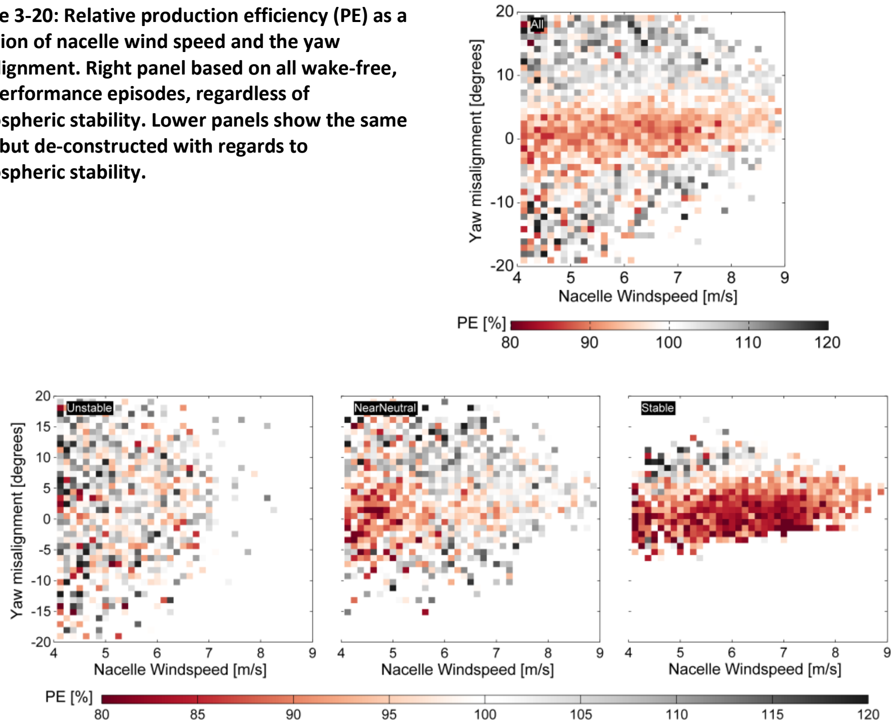

3.3 DISCUSSION & CONCLUSIONS

The results in section 3.2.1 and 3.2.2 is not universal. They depend on the site and on the weather conditions present during the analysed period. Since the period analyzed only contains a few wind speeds above the rated wind speed, the conclusions below are thus mainly applicable for wind speeds below rated wind speed.

This is also why no mathematical relationships relating vibrations and ambient variables are presented.

It is not straight forward to quantify the contribution of the different ambient conditions to the total vibration level and how they influence the production efficiency. The different variables related to the ambient conditions are also related to each other, making it even more difficult. More sophisticated techniques, like principal component analysis or multivariate regression analysis might be able to get more insight into the relationship between the ambient conditions and the vibration level/production efficiency.

However, in terms of the how the vibrations and the relative production efficiency (PE) are influenced by the ambient conditions the results indicate the following:

- There is a tendency that vibrations increase with increased wind speeds, this relationship is more pronounced in unstable and near-neutral conditions compared to stable atmospheric conditions.
- With increased atmospheric stability the PE typically becomes lower.

- Increased atmospheric stability is typically associated with increased vertical wind shear and less turbulence. The data in this analysis support this.
- Suppression of turbulence with increasing atmospheric stability seems to be the main explanation why the unstable/stable classification is associated with higher/lower PE than normal.
- Yaw misalignment is considerably smaller in the stable conditions compared to when the stability is classified as near-neutral and unstable. This is likely related to that the control system is working better when the flow becomes less turbulent. A smaller yaw misalignment is expected to be associated with larger production efficiency, however in this case the negative effect on the PE from less turbulence and higher wind shear during stable conditions dominates the effect of smaller yaw misalignment.

Worth emphasizing is that the relative production efficiency is based on the actual production of the WT and a value below/over 100 % **does not imply that the WT is under-/over-performing relative to a specific power curve**.

In the analysis of the relative production efficiency 1-minute statistics is used instead of the 10-minute statistics, which is the standard in the wind power community. The sole reason for this is to increase the amount of data going into the analysis. By using 1-minute statistics compared to the 10-minute statistics synchronization issues between the ZDM (measuring at 200 m up-stream of the rotor) and SCADA measurements becomes more prominent. The travel time for a parcel of air from the ZDM measurement range of 200 m to the nacelle at 6 m/s is more than 30 seconds. We have not accounted for this in the analysis and this might impact our results.

3.4 FUTURE WORK

There are several things not examined in detail that is proposed for future work

- The low level vibrations in the lateral that are more or less constant for a wide range of ambient conditions should be analysed in future projects to establish if it is an anomaly in the measurements or if it is a real feature.
- The standard deviation is a rather rough estimate of the vibration level. Signal processing is a whole research field of its own and it is highly likely that there are tools within that field of research that could be very useful in the analysis of the vibration data in future projects.
- The turbulence intensity is probably not the best characterization of the turbulence when the vibrations in the nacelle are studied. High frequency measurements with ultra sonic instruments in future projects and measurement campaigns could be used to shed light over the size of the turbulence elements during different atmospheric conditions.
- More sophisticated techniques, like principal component analysis or multivariate regression analysis might be able to shed more light into the relationship between the ambient conditions and the vibration level/production efficiency.

4 Transient wind flow simulations over non-homogeneous forest on complex terrain.

4.1 MOTIVATION

The motivation and objective for the performed work is to verify state-of-the-art simulation methods used in microscale modelling of wind farms in complex sites. The complexity of an advanced flow model that comprises variations such as different ground elevation, terrain roughness (open water to forest) in combination with turbine modelling is very high. LES modelling of forested areas is today very novel but is starting to be a realistic choice in research applications. However, there is a great need for validation. In this project, measurements have been performed to assess the local flow properties inside a farm located in a complex forested site. This is done in preparation for the future inclusion of rotor modelling. To couple an advanced flow model for this purpose in combination with accurate turbine modelling is a very large challenge. The validation of the model, to represent the wind over forest, is a fundamental step towards an accurate computation of wake interaction inside wind farms.

4.2 ANALYSIS OF PERFORMED MEASUREMENTS

As described in Chapter 2, two nacelle mounted lidars was installed at the LoadMonitor site. Since high frequency raw data was available from the ZDM, that was deemed the most promising for comparing the measured and simulated wind speed.

Lidars measure the Doppler shift of the frequency of the emitted laser beam and calculated the wind speed according to the following equation:

$$u_r = \frac{1}{2}\lambda\Delta f$$

where λ is the wavelength of the emitted laser beam and Δf is the Doppler frequency shift. Since the frequency only shifts due to movements in the direction of the beam it is only possible to measure the LOS velocity, u_r. If the wind field is homogenous one can determine the wind speed in the direction of the wind turbine, but since the site is complex we instead opted to compare the u_r estimates directly since that is readily computed from the simulated wind field. From the LES results it is possible to estimate the error in mean wind speed estimation, $u(z)$, from the instantaneous values of u_r since the whole wind field is known. In the following section we therefore show both the true mean wind speed in the mean wind direction and the estimation based on the line of sight velocity for the LES results.

The raw data output of the ZDM consists of fast Fourier transformed (fft) backscatter signal, information of the beam angle and the estimated Line of Sight velocity, u_r. When examining the raw data output of the ZDM, periods of noise in the fft signals were detected and to have as much control as possible of the estimated u_r a filter method was developed to determine a new estimate of u_r from the fft signal. The routine loosely follows the recommendations by Mann et al. (2010) and Branlard et al. (2013), which showed that the velocity distribution of a wind field could be well approximated by the average fft spectra of a continuous wave lidar and that the average wind speed is better estimated by the average spectra than from averaging high frequency u_r estimates. The developed method consists of the following steps:

- Divide the scan into twelve sectors of 30° width, centred at 0°, 30°, 60°etc.
- For each revolution of the laser, average the fft spectrums for all returns falling within each of the twelve sectors.
- Remove all backscatter for frequencies corresponding to lower wind speed than 1.65 ms^{-1} in order to remove the backscatter due to blade passage.
- Compute the centroid of the spectrum and the standard deviation as the rms of the deviations from the centroid.
- Repeat the above step, but only for data falling within ±2 standard deviations from the centroid values. The centroid value is then saved as the wind speed u_r and the standard deviation as σ_{ur}.

The last step removes round 1.5 % of the original variance if the measurement contains no noise, but was added since the centroid calculation is very sensitive to noise on frequencies corresponding to very high wind speeds. The last step proved effective in limiting that source of error. Figure 4-1 shows an example of the routine described above. It shows the distributions from each of the twelve sectors together with their centroids, u_r, and the mean of the twelve individual radial wind speeds as a black line.

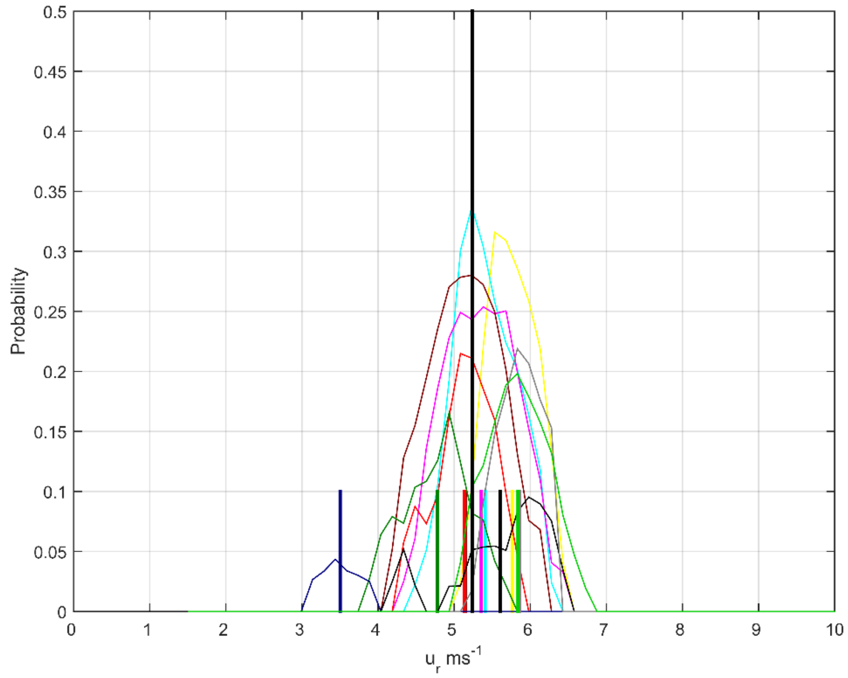

Figure 4-1: Velocity distributions for different phases of the lidar scanning circle. Mean wind speeds for each phase is marked by vertical lines. The mean of the entire circle is marked by a black line.

The wind speed distributions in each of the twelve sectors were then averaged to compare with the distributions from the modelled wind field.

By averaging the distributions, instead of making distributions of the u_r estimates as outputted from the instruments, it is possible to retain more influence from the small scale structures of the wind field. At a distance of 200 m, the line averaging due to non perfect focus of the lidar beam removes most of the variations on time scales less than a minute (Simley et al., 2012). While this may not be a problem when studying the rotor equivalent wind speed, it is a large problem for flow model validation. Following Mann et al. (2010) we instead averaged the Doppler spectrums/wind distributions to retain the information in the spectrum tails stemming from the small scale variations.

The lidar signal to noise ratio was considerably better for the uppermost sections of the scan (when the beam is pointing upwards). This had as an affect that more data was collected from the upper sections of the scanning circle. Based on the above division into twelve sectors the data coverage for the periods later used in the LES validation is shown in Table 4.1.

Table 4.1 Data coverage in different phases of the scanning circle of the Zephir lidar

Sector center (degrees)	0	30	60	90	120	150	180	210	240	270	300	330
Data coverage (%)	69	68	66	65	54	35	4	32	1	62	65	68

4.2.1 Data selection

In order to validate the LES a direction without influence from upstream turbines was selected. The reason to not average in all directions without upstream wakes is that since the LES model contains the actual forest coverage and density as well as the topography, the upstream flow varies with direction. For the validation, the lidar running in Config 3 (see Section 2.2.2) was chosen, which means that the distance from the nacelle to the wind measurements was 200 m. Since the opening angle is 30 degrees of the lidar, the radius of the cone is 53.6 m at 200 m distance. That has the effect that sometimes one side of the scan is affected by wakes while the other is not, which will cause the lidar internal routine to show that the wind direction is different than it is. Comparing the lidar wind direction with the yaw thus enables identification of when part of the scan is affected by wakes, and one can then determine sectors where there is no influence from the wakes. This analysis was done using Figure 2-15 and the sector 255 ± 12.5 degrees was identified as the undisturbed sector with the most measurements.

Since the LES was run with a constant geostrophic wind speed, it requires that the wind speed from the measurements is stationary, since otherwise the distributions will widen considerably. In order to ensure that, 10 minute averages of the fft spectra were used when comparing to the LES, rather than 30 minute, or 60 minute time series, which would be more likely to contain shifts in wind direction or mean wind speed.

In order to compare the measurements to the LES results, the same conditions that were modelled must also be filtered for in the measurements. Since the stratification in the model is neutral, it is key to filter out neutral conditions in the measurements to judge the validity of the modelled results. Two attempts were done to do that. First, periods that had been modelled to be neutral in the meso-scale simulations were labelled as neutral (see Section 2.5.2). Second, periods between 05:00-10:00 and 17:00-20:00 local time was considered to represent neutral conditions. Since morning and evening can be considered as a transition time between stable conditions during night and unstable conditions during day, these periods usually approximate neutral conditions. This second criterion was used in order to filter for more strictly neutral periods than obtained by the WRF classification.

Since not only mean wind speed, but also turbulence is a part of the comparison, the selection of a narrow wind speed interval, matching the modelled wind speed, is necessary. This was achieved by selection of data ±0.5 ms^{-1} of the modelled wind speed at hub height. After all the above steps were performed the data had been narrowed down to

- **103** 10 min periods if only wind speed and direction were considered
- **70** 10 min periods when wind speed, wind direction and WRF stratification was considered
- **10** 10 min periods when wind speed, wind direction and morning/evening neutral selection was applied

4.2.2 Verification of model results

Since the measurement site did not have a meteorological mast, the model was first validated against measurements from the Ryningsnäs tower (Arnqvist et al., 2015). Three different sectors were modelled, 100°, 240° and 290°. Although all sectors were predominately forested, the upwind conditions differ between the sectors in the scale of the heterogeneity and the height, density and age of forest of the forest stands. This was done to test if the model could accurately reproduce variations due to different upstream conditions. Laser scans were downloaded and prepared as described in Section 2.4.3.

Figure 4-2 shows the results from the three different sectors in terms of wind speed, turbulence kinetic energy (TKE) and wind direction. Measurements were treated as described in Arnqvist et al. (2015). Since the model is currently only able to simulate neutral conditions, the sonic anemometers where used to filter the heat flux ensuring only measurements representing neutral conditions were chosen.

It was found that in order to accurately reproduce the measurements, a very large domain with detailed information of the forest characteristics as well as terrain height was necessary. The upstream effects in rotor height seem to be influenced by upstream effects more than 10 km away.

The results of the study are very promising; the model was able to reproduce the characteristics of both the wind and TKE profiles, and how these characteristics changed with direction. In Figure 4-2a the wind profile is shown. The profiles from the three different directions are very similar, but differ in the lower part, due to effects of the near forest, and even though the LES model predicts larger effects than the measurements, the trend is the same. The TKE profile is shown in Figure 4-2b and also here the trends are captured by the model. The level of TKE is generally higher in the measurements, which to some extent may be explained by the absence of the fine scale structures in the wind field missing due to the limited cell resolution in the LES, particularly in the vertical direction. It is interesting to note though, that the relative level of TKE changes in the different directions and the change is the same in the modelled wind. Also the decrease with height is well captured, 290° having a steeper decrease than 240° in both measurements and modelled wind.

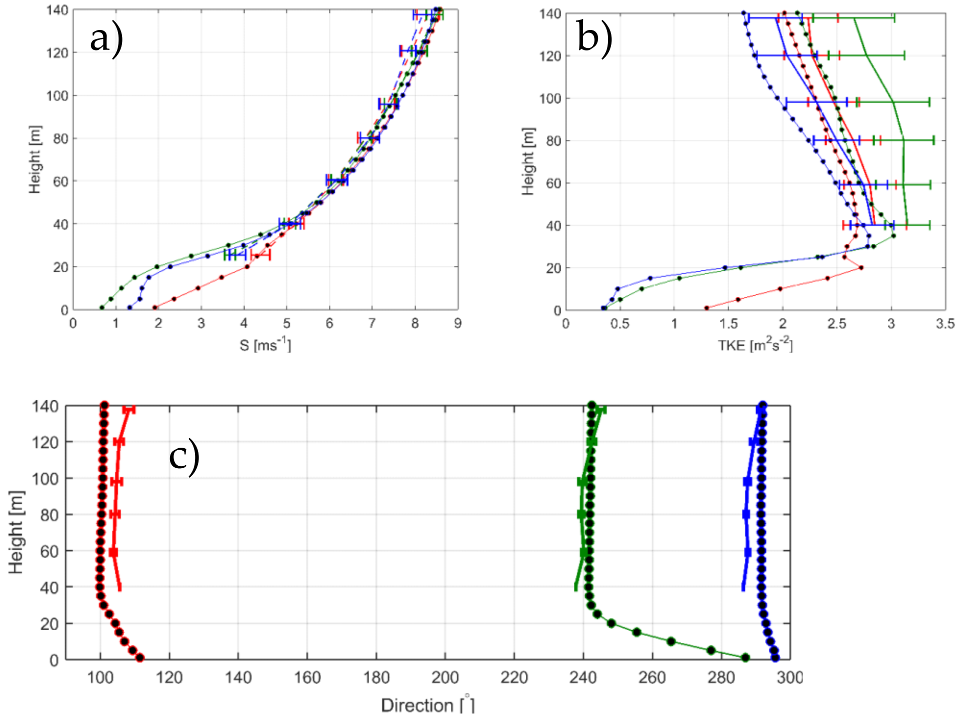

Figure 4-2: Comparison of the LES with the measurements from Ryningsnäs. Red curves from 100°, green curves from 240° and blue curves from 290°. The measurements are shown by full lines and error bars, corresponding to the 95 % confidence of the mean. The LES results are shown in full lines with filled black markers

4.2.3 Velocity field over forest

The wind flow around the location of the lidar is computed with LES within the computational domain described in Sec. 2.4.3. Figure 4-3 to Figure 4-8 and Figure 4-9 to Figure 4-14 are shown to illustrate the variation of the mean velocity and total TKE (resolved plus subgrid), respectively, in correspondence to the topography of the terrain (Figure 2-8) and the PAD distribution (Figure 2-9 to Figure 2-12). It can be appreciated that differences in ground elevation have a larger impact in the velocity field at hub heights than foliage. The Figure 2-8 (ground elevation) displays a central, two-branch structure where the height is the lowest (about 100 m) of the simulated terrain, corresponding to agricultural fields in the valley, where the mean velocity above is noticeably higher up to 40 m. These regions also correspond to higher levels of TKE although these prevail for shorter heights (until 20 m). The highest levels of TKE seem to be reached at about 40 m and therefore above the forest canopy, which evidences the effect of the trees in the turbulence increase.

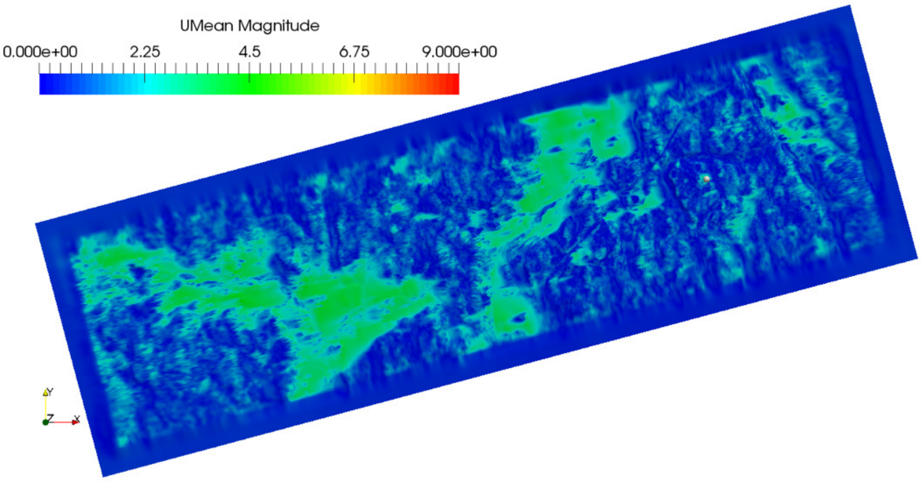

Figure 4-3: Average velocity magnitude (in m/s) at 1 m from the ground.

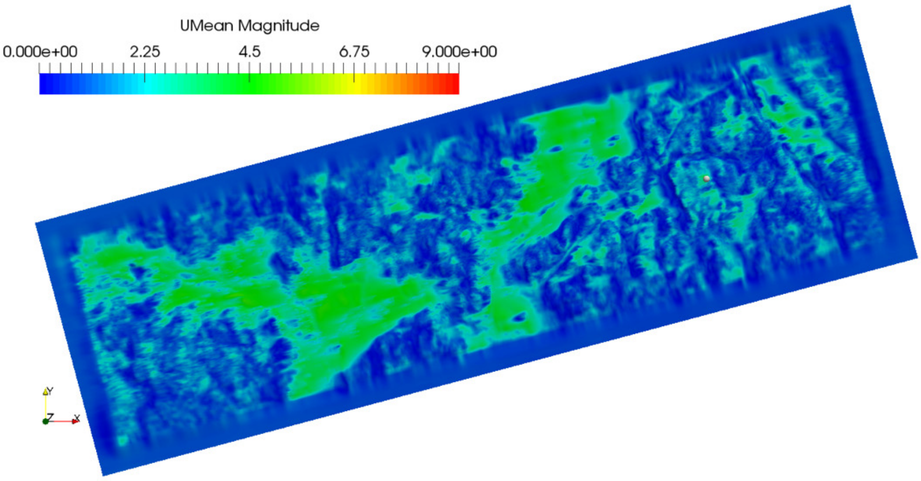

Figure 4-4: Average velocity magnitude at 5 m from the ground.

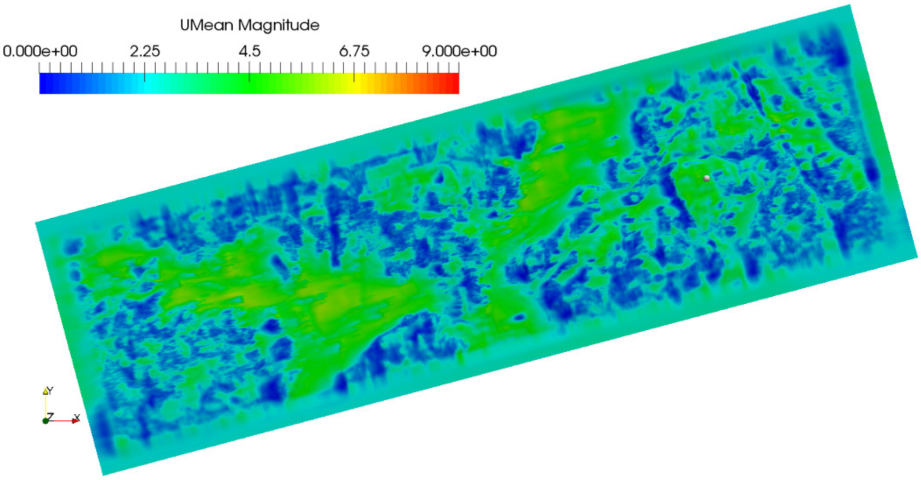

Figure 4-5: Average velocity magnitude at 15 m from the ground.

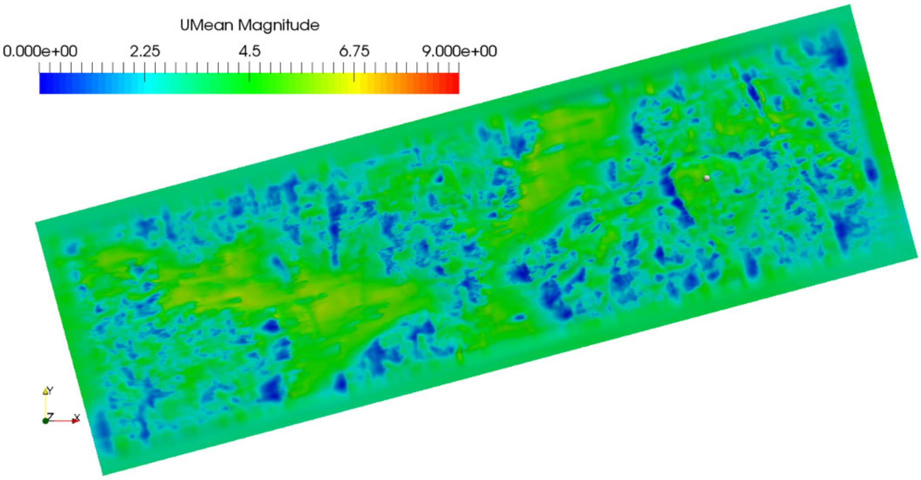

Figure 4-6: Average velocity magnitude at 20 m from the ground.

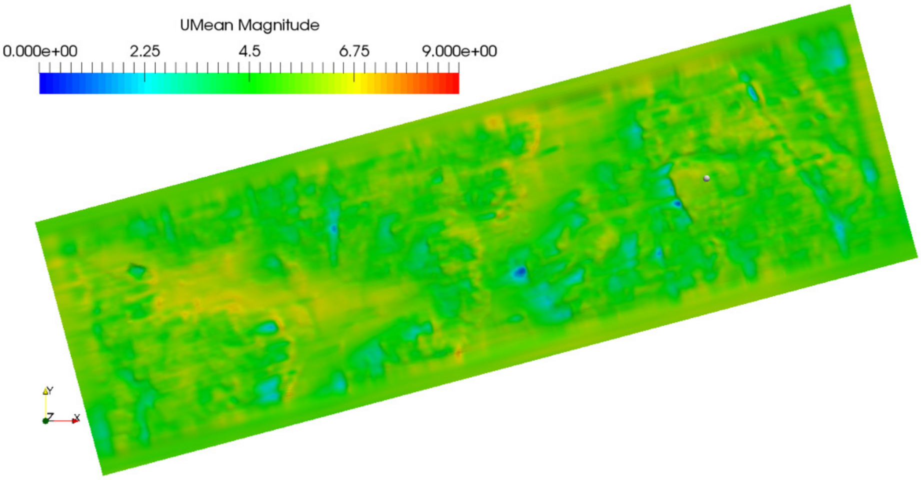

Figure 4-7: Average velocity magnitude at 40 m from the ground.

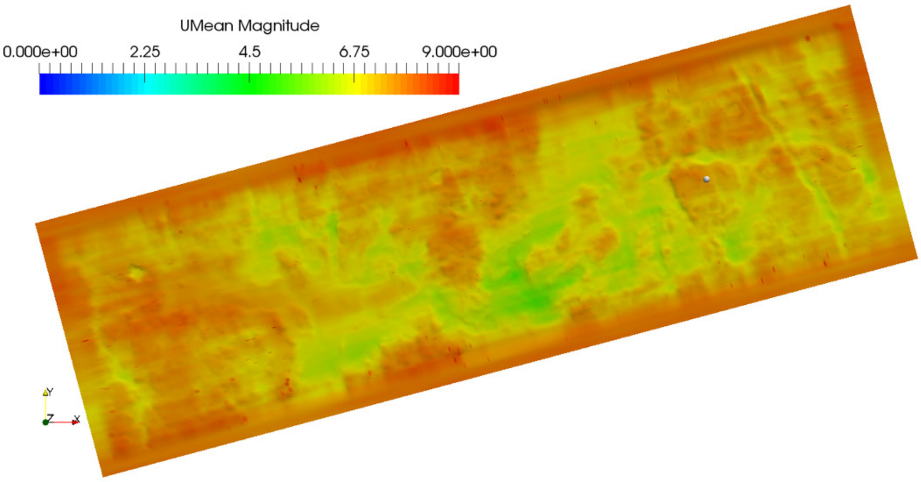

Figure 4-8: Average velocity magnitude at 100 m from the ground.

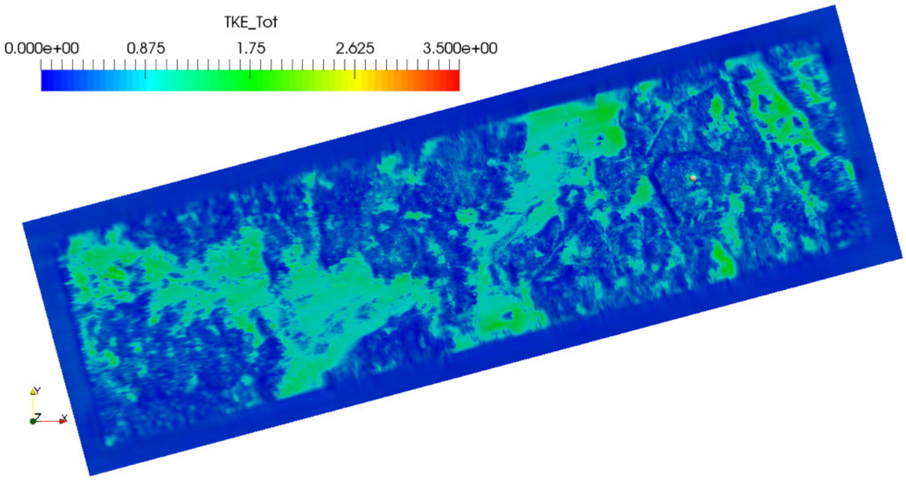

Figure 4-9: Turbulence kinetic energy (in m^2/s^2) at 1 m from the ground.

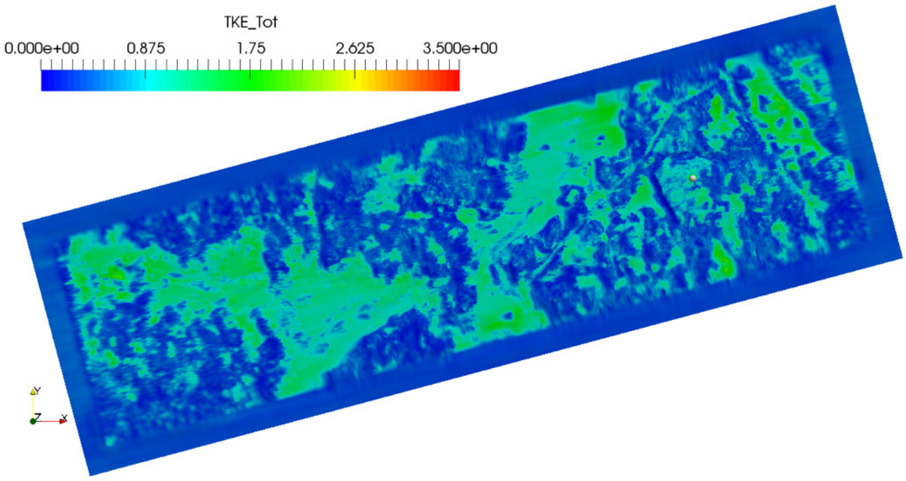

Figure 4-10: Turbulence kinetic energy at 5 m from the ground.

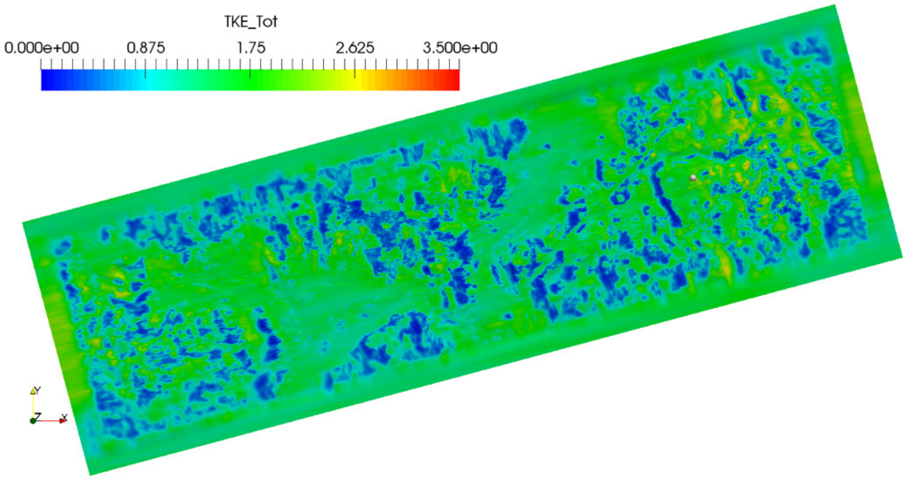

Figure 4-11: Turbulence kinetic energy at 15 m from the ground.

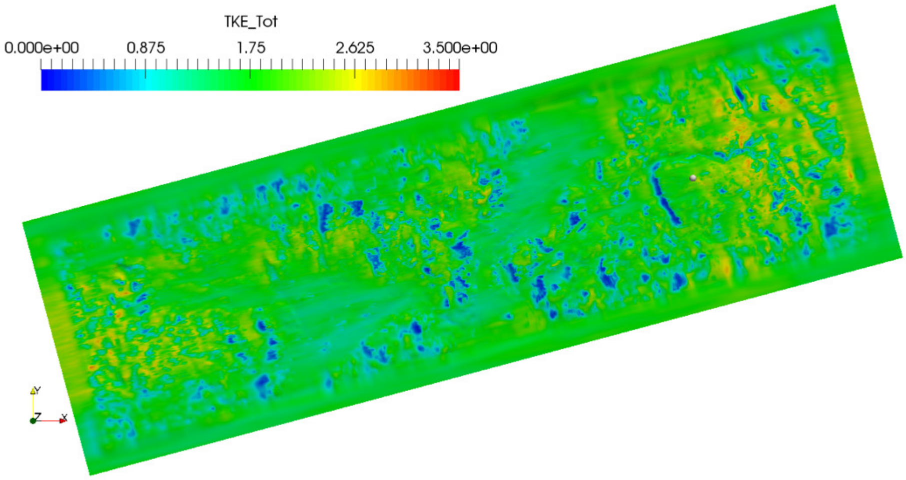

Figure 4-12: Turbulence kinetic energy at 20 m from the ground.

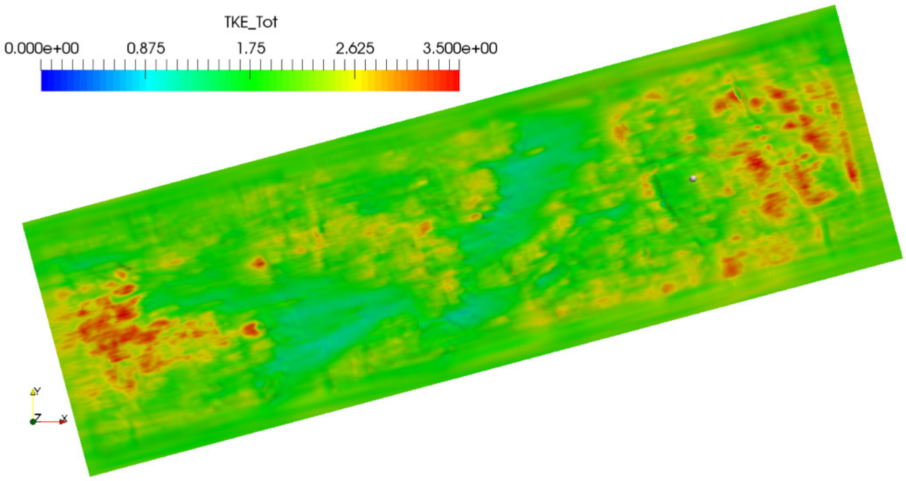

Figure 4-13: Turbulence kinetic energy at 40 m from the ground.

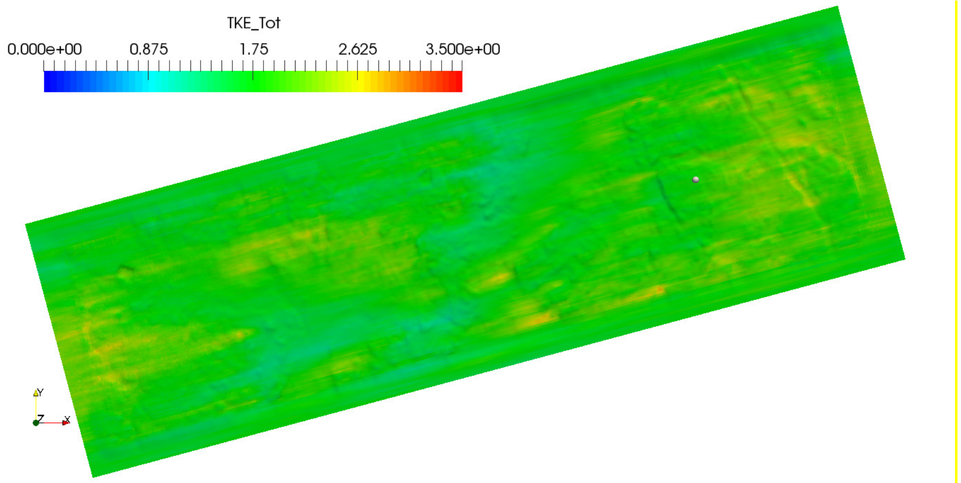

Figure 4-14. Turbulence kinetic energy at 100 m from the ground.

4.2.4 Comparison between measurement and model results

Following Mann et al. (2010), Branlard et al. (2013) and Sathe & Mann (2013) the variables most straight forward to compare, and with the highest confidence, is the mean wind speed and the mean distributions of the ZDM.

Since the line averaging due to inexact focus of the laser beam may be considerable at the distance of comparison (200 m, Simley et al. 2012), averaging of the LES results were first done in three adjacent grid points in the direction of the beam, corresponding to a focal length of 30 m, although it was later noted that this had negligible small impact on the final results. The mean wind speed from the ZDM and the LES is shown in Figure 4-15. The wind profile is shown as function of the distance from the hub of WT4. The lidar was focused on 200 m upstream of the WT, so at that position the same velocity components as measured by the ZDM were sampled from the LES. To facilitate the highest possible confidence in the validation data, the LES results were transformed into the coordinate system of the ZDM. This also enabled an estimation of the error introduced by assuming homogenous flow since these components, u_r from the LES, can be averaged and transformed into mean horizontal wind speed as you would with the u_r from the ZDM. This is done according to:

$$\bar{u} \approx \overline{u_r} / \cos(\alpha_o/2)$$

Where the over bar represents time average and α_o is the opening angle of the lidar (in this case 30°).

The curves corresponding to this procedure are shown in yellow and dotted black in Figure 4-15, and although there is some difference between the left and the right side of the scanning circle (most likely due to wind veer) the error is small.

What is also apparent from Figure 4-15 is that the wind speed at hub height is very similar at 200 m upstream, 100 m upstream and at the WT4 position, but that some differences stemming from variations in ground elevation and forest cover can be seen further down.

Comparison between the simulations and the measurements show that using all the wind measurements yields a much higher wind shear in the measurements compared to the LES. By filtering only for time stamps belonging to morning and evening transition periods, labeled as *neutral hours* the shear becomes much more similar. Using the WRF classification for neutral show a wind shear that is very similar to the wind shear using all the data. This may be an indication of that the stability criterion used with the WRF data may be too broad to filter out strictly neutral data, biasing the results slightly towards stable stratification, but there may also be some uncertainty introduced since the WRF filtering is based on modelled and not observed stratification. What can, in addition, be seen from the measured wind profile filtering for *neutral hours* is that the wind speed is higher in the right side of the scan that in the left. This may be either due to a yaw misalignment of the turbine or due to bias from noise in the measurements. The large difference at hub height is due to noise that can also be seen effecting the distribution in Figure 4-16.

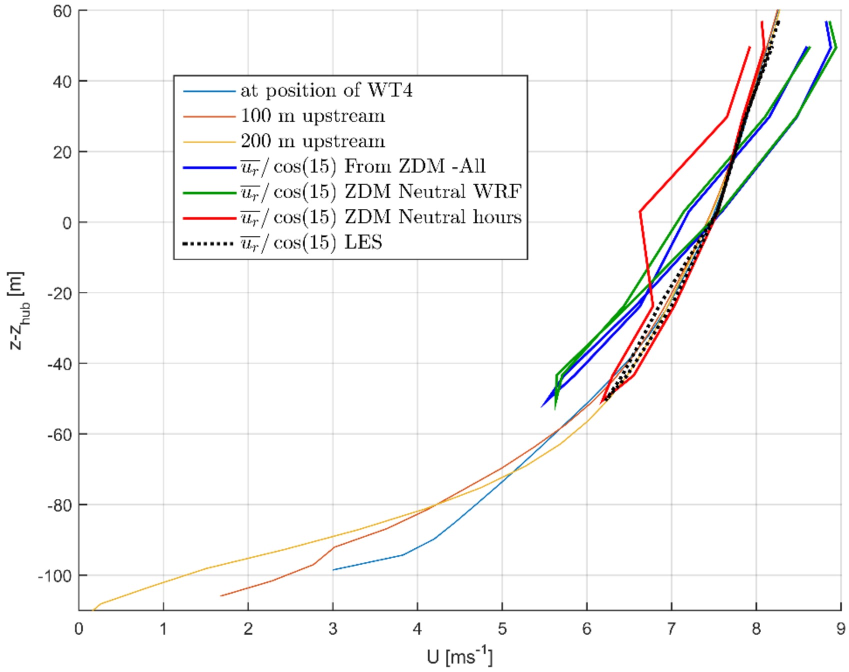

Figure 4-15: Mean wind speed from the LES and the ZDM.

Figure 4-16 shows the distributions from the twelve phases of the scanning circle for the conditions described above. The centroids of these distributions correspond to the wind speed profiles shown in Figure 4-15. The distributions further indicate that the wind speed profiles using all the data and the data labeled neutral by WRF may be biased towards stable stratification since these distributions are narrower than the distribution from using transition periods. All of the measured distributions show noise in varying degree, but it is only for the phase 270° that the noise affects the mean wind speed estimation, and due to the lower number of measurements the highest effect is seen for the *neutral hours* data filtering. Over all the agreement between the LES and the data filtered for neutral conditions using *neutral hours* is good and the LES seems to represent the measured flow accurately.

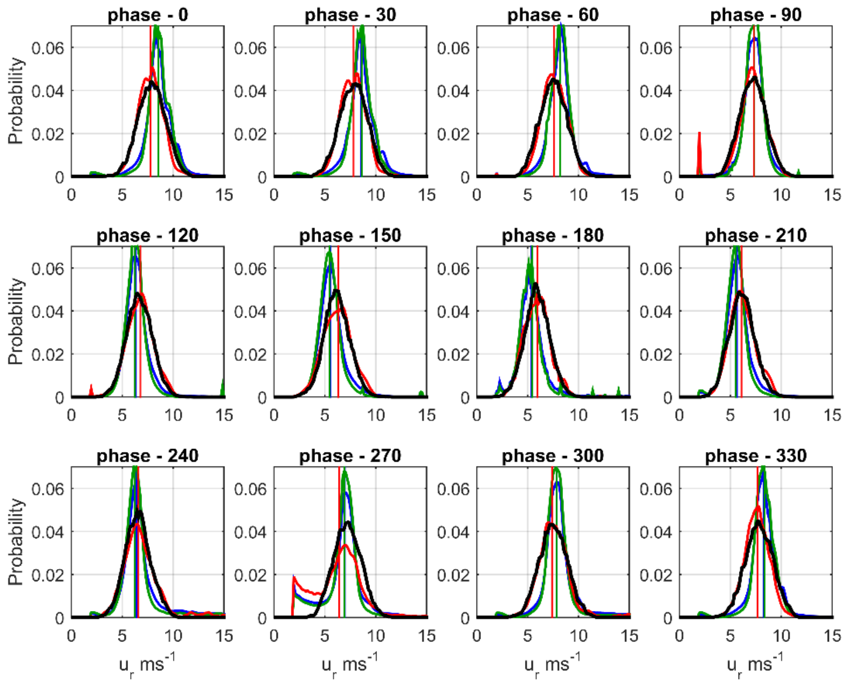

Figure 4-16: Wind speed distributions from the LES and the ZDM. The same color coding as in Figure 4-15 is used.

4.3 CONCLUSIONS & FUTURE WORK

- It is shown that LES is capable of reproducing the variability of the flow over the non-homogeneous forest and complex terrain. In particular, that the distribution of velocity fluctuations estimated by the LES compares favourably to that computed form the lidar measurements, at the given mean velocity and stability condition.
- Since the methodology to model the forest and terrain takes into account local variations in roughness and differences in the distribution of canopy density, it will be possible to study the effects that such variations impose on the wake interaction and, in general, on the prediction of the production of the wind park. This is important to note in the context of CFD modelling, as some techniques commonly employed do not include transient effects (e.g. RANS) which are fundamental for the representation of turbulence fields in wakes, or disregard the local variations of vegetation and topography.
- The comparison of the CFD results with the measurements is sensitive to the selection of data of corresponding stability conditions. Since the LES computations are based on an incompressible solver, the selection of measurements in neutral conditions is crucial for the comparison.

- Based on this study it will be possible to assess full wake interaction of wind farms located in forested and complex terrain sites. This is achieved by combining the developed flow model with available rotor models previously developed within the Nordic consortium. This way, state-of-the-art modelling of wake interaction inside wind farms in heterogeneous forest and complex terrain will be achieved. An article including this work is currently in preparation.

5 Bibliography

Arnqvist, J., Segalini, A., Dellwik, E., & Bergström, H. (2015). Wind Statistics from a Forested Landscape. *Boundary-Layer Meteorol, 156*(53), https://doi.org/10.1007/s10546-015-0016-x.

Arya, S. P. (2001). *Introduction to Micrometeorology, Second edition.* Academic Press.

Bardal, L., Sætran, L., & Wangsness, E. (2015). *Performance test of a 3MW wind turbine - Effects of shear and turbulence.* Department of energy and process engineering, NTNU, Presented at 12th Deep Sea Offshore Wind R&D Conference, EERA DeepWind'2015.

Bechmann, A. (2006). *Large-Eddy Simulation of Atmospheric Flow over Complex Terrain.* Roskilde, Denmark : PhD thesis, Risø Technical University of Denmark.

Bergström, H., Alfredsson, H., Arnqvist, J., Carlén, I., Dellwik, E., Fransson, J., . . . Söderberg, S. (2013). *Wind Power in Forest, Elforsk Report 13:09.*

Blodau, T. (2013). *Review of Inner/Outer Range Proposal.* Presented at 3rd meeting of the Power Curve Working Group.

Boudreault, L.-É. (2015). *Reynolds-averaged Navier-Stokes and Large-Eddy Simulation Over and Inside Inhomogeneous Forests.* Ph.D. Thesis Technical University of Denmark, Department of Mechanical Engineering.

Boudreault, L.-E., Bechmann, A., Taryainen, L., Klemedtsson, L., Shendryk, I., & Dellwik, E. (2015). A LiDAR method of canopy structure retrieval for wind modeling of heterogeneous forests. . *Agricultural and Forest Meteorology, 201*, 86-97, DOI: 10.1016/j.agrformet.2014.10.014.

Branlard, E. P., Fischer, A., Mikkelsen, T., Harris, M., Slinger, C., & Montes, B. F. (2013). Retrieving wind statistics from average spectrum of continuous-wave lidar. *Atmos. Meas. Tech., 6*, 1673-1683, https://doi.org/10.5194/amt-6-1673-2013.

Burton, T. S. (2001). *Wind Energy Handbook.* John Wiley & Sons.

Carlén, I. (2017). *Elforsk report - Load Monitor:Measuring and modeling vibrations and loads on wind turbines. Part 2: Concepts for monitoring loads on towers and foundations.*

Churchfield, M. J. (2014). Adding complex terrain and stable atmospheric condition capability to the OpenFOAM-based flow solver of the simulator for on/offshore wind farm applications (SOWFA). *ITM Web of Conferences Vol. 2.* EDP Sciences.

Cosack, N. (2010). *Fatigue loading monitoring with standard wind turbine signals.* PhD Thesis, University of Stuttgart.

Dee, D. P. (2011). The ERA-Interim reanalysis: configuration and performance of the data assimilation system. *Q. J. R. Meteorol. Soc.*

Derrick, A., & Oram, A. (2014). *Illustrating the Importance of Site Specific PC.* Presented at 6th meeting of the Power Curve Working Group.

DNV GL. (2016). *Bladed Software*.

EMD International A/S. (2015). *WindPRO 3.0 User Manual, Loads*. Retrieved from http://help.emd.dk/knowledgebase/content/WindPRO3.0/05-UK_windPRO3.0-LOADS.pdf

Gancarski, P., & Chávez-Arroyo, R. (2014). Meshing procedure for the atmospheric wind flow modelling. *2nd Symposium on OpenFOAM in Wind Energy.* Boulder, Colorado, USA.

Hansson, J., Lindvall, J., & Byrkjedal, Ø. (2016). *Energiforskrapport - Quantification of icing losses in wind farms.* Energimyndigheten.

Holierhoek, J. K. (2010). *Recommended Practices for Measuring in Situ the 'Loads' on Drive Train, Pitch System and Yaw System.* Protest ECN-E--10-083.

Holtslag, M. C., Bierbooms, W. A., & van Bussel, G. J. (2014). Estimating atmospheric stability from observations and correcting wind shear models accordingly. *Journal of Physics: Conference Series. Volume 555, conference 1.* IOP Publishing Ltd.

Højstrup, J. (2014). *Increased energy production by optmisation of yaw control.* VGB PowerTech International Journal for Electricity and Heat Generation.

IEA Wind Task 32. (2015). *Task 32 Textension for Proposal.*

IEA Wind Task 32. (2016). Retrieved from The International Energy Agency (IEA) Wind, Task 32 - Lidar: http://www.forwind.de/IEAAnnex32/

IEC 61400-1. (2005). *International standard, Wind turbines - Part 1: Design requirements.* IEC.

IEC 61400-12-1. (2005). *International standard Wind turbines - Part 12-1:Power performance measurments of electricity producing wind tubines. First edition.* IEC.

IEC 61400-12-1 Ed.2. (2017). *International standard Wind turbines - Part 12-1:Power performance measurments of electricity producing wind tubines. 2nd edition.* IEC.

IEC 61400-13. (2001). *International standard, Wind turbines - Part 13: Measurement of mechanical loads.* IEC.

IEC TC 88. (2016). *IEC Technical Committee*. Retrieved from International Electrotechnical Commission (IEC) Website: http://www.iec.ch/dyn/www/f?p=103:7:0::::FSP_ORG_ID,FSP_LANG_ID:1282,25

Ivanell, S., Carlen, I., Nilsson, K., Sarmast, S., Odemark, Y., Andersen, S., . . . Henningson, D. (2013). *Optimization of Large Wind Farms - The Nordic Consortium, Activity report 2009-2012.* Elforsk rapport nr: 13:12.

Klemp, J. B., Skamarock, W. C., & Dudhia, J. (2000). *Conservative split-explicit time integration methods for the compressible non-hydrostatic equations.* see http://www.wrf-model.org/. Retrieved from http://www.wrf-model.org

Koopman, F. (2013). *Accelerating Wind Energy: A physical approach to monitor tower base fatigue loads using standard signals.* MSc Thesis, Delft University of Technology.

Larsen, T. J. (2008). *HAWC2Aero, the user's manual Tecnical Report Risø-R-1631(ver.1-0)* .

Lindvall, J., Hansson, J., & Undheim, O. (2016). *Energiforskrapport - Post-construction production assessment of wind farms.*

Lundquist, J. K. (2010). *Atmospheric Stability Impacts on Wind Turbine Performance.* presented at Wind Energy R&D Workshop at NCAR.

Mann, J., Peña, A., Bingöl, F., Wagner, R., & Courtney, M. (2010). Lidar Scanning of Momentum Flux in and above the Atmospheric Surface Layer. *J. Atmos. Oceanic Technol., 27*, 959-976, https://doi.org/10.1175/2010JTECHA1389.1.

Manwell, J. M. (2010). *Wind Energy Explained: Theory, Design and Application, Second Edition.* John Wiley & Sons Ltd.

Michalakes, J., Chen, S. D., Hart, L., Klemp, J., Middlecoff, J., & Skamarock, W. (2001). *Development of a Next Generation Regional Weather Research and Forecast Model.* Singapore: Eds. Walter Zwieflhofer and Norbert Kreitz. World Scientific.

Nebenführ, B. (2015). *Turbulence-resolving simulations for engineering applications.* Gothenburg, Sweden: Ph.D. thesis, Chalmers University of Technology.

Obdam, L. R. (2009). *Flight Leader Concept for Wind Farm Load Counting: First offshore implementation.* Energy Research Centre of the Netherlands, ECN-M--09-114.

PCWG-1. (2016). Retrieved from Power Curve Working Group Website: http://www.pcwg.org/

PCWG-2. (2016). *1st Intelligence Sharing Initiative Definition Document (PCWG-Share-01).*

PCWG-3. (2016). *Power Curve Working Group 2016 Roadmap.*

Rareshide, E., Tindal, A., Johnson, C., Graves, A. M., & Simpson, E. (2009). *Effects of complex wind regimes on turbine performance.* Scientific Proceedings, American Wind Energy Association WINDPOWER Conference (Chicago, IL).

Sathe, A., & Mann, J. (2013). A review of turbulence measurements using ground-based wind lidars. *Atmos. Meas. Tech., 6*, 3147-3167, https://doi.org/10.5194/amt-6-3147-2013.

Schlipf, D., Kapp, S., Anger, J., Bischoff, O., Hofsäß, M., Rettenmeier, A., . . . Kühn, M. (2011). *Prospects of optimization of energy production by LIDAR assisted control of wind turbines.* Brussels: European Wind Energy Association Annual Event (EWEA).

Schumann, U. (1975). Subgrid scale model for finite difference simulations of turbulent flows in plane channels and annuli. *Journal of computational physics, 18*, 376-404.

Simley, E., Pao, L., Kelley, N., Jonkman, B., & Frehlich, R. (2012). LIDAR Wind Speed Measurements of Evolving Wind Fields,. *50th AIAA Aerospace Sciences Meeting including the New Horizons Forum and Aerospace Exposition, Aerospace Sciences Meetings, https://doi.org/10.2514/6.2012-656.*

Skamarock, W. C., Klemp, J. B., Dudhia, J., Gill, D. O., Barker, D. M., Duda, M. G., . . . Powers, J. G. (2008). *A Description of the Advanced Research WRF Version 3.* Boulder, U.S.: NCAR.

Stull, R. B. (1988). *An introduction to Boundary Layer Meteorology.* Dordrecht: Kluwer Academic Publishers.

Svenningsen, L. T. (2015). *A new approach to fast and accurate site suitability assessment.* Brazil Windpower 2015 Conference and Exhibition.

Turkyilmaz, U., & Undheim, O. (2016). *Energiforsk Report - Assessment and optimization of the energy production of operational wind farms. Part 2: Use of remote sensing for performance optimization.*

UniTTe. (2016). *UniTTe - Unified Turbine Testing*. Retrieved from http://www.unitte.dk/Project-Overview/Summary

Wagner, R. (2010). *Accounting for the speed shear in wind turbine power performance measurement.* PhD Thesis, Risø DTU.

Vanderwende, B. J., & Lundquist, J. K. (2012). The modification of wind turbine performance by statistically distinct atmospheric regimes. *Environmental Research Letters*.

Veldkamp, H. F. (2006). *Chances in Wind Energy: A Probabilistic Approach to Wind Turbine Fatigue Design.* PhD thesis Delft University of Technology.

Yoshizawa, A. (1986). Statistical theory for compressible turbulent shear flows, with the application to subgrid modelling. *The Physics of Fluids, 7*(29).

6 Appendix A - Desktop study: load assessment and load monitoring of wind turbines

The modern wind turbines are designed to perform and produce energy throughout their lifetime typically 20 years. As a result of operation under site specific conditions, the wind turbine components are subject to various complex dynamic forces or loads. Manwell et al categorize the wind turbine loads into five (Manwell, 2010):

- Steady loads
- Cyclic loads
- Stochastic loads
- Transient loads
- Resonance-induced loads

The IEC standard 61400-1 (IEC 61400-1, 2005) and Burton et al (Burton, 2001) specify the load sources in below categories:

- Aerodynamics
- Gravitational and inertial forces
- Actuation system (operation and control)
- Other loads such as wakes, icing, etc

The structural design process can become very complicated when all these loads and their sources are taken into account. Therefore, a set of specific load cases have been introduced by the IEC standards, which are widely used in the type certification of the wind turbines today. The IEC standard 61400-1 classifies design load cases (DLC) by turbine operation (IEC 61400-1, 2005):

1. Power production
2. Power production plus fault
3. Start up
4. Normal shut down
5. Emergency shut down
6. Control failure or network failure
7. Parked (standing still or idling state): e.g including extreme yaw misalignment
8. Transport, assembly, maintenance and repair

Some of the DLCs are divided into sub categories based on wind conditions which are briefly:

- Normal wind conditions: such as normal turbulence model (NTM), normal wind profile model (NWP)
- Extreme wind conditions: such as extreme coherent gust with direction change (ECD), extreme direction change (EDC), extreme operating gust (EOG), extreme turbulence model (ETM), extreme wind shear (EWS).

All these wind conditions are analyzed through either fatigue (F) strength or ultimate (U) tensile strength with safety load factors defined in the IEC standard.

As outlined by Veldkamp (Veldkamp, 2006), a generic wind turbine design procedure starts with the calculation of loads and then follows the validation process with measurements. The procedure of measurement of loads is described in the IEC standard 61400-13 (IEC 61400-13, 2001). The main load quantities considered in the IEC standard 61400-13 are presented by Holierhoek et al (Holierhoek, 2010), Table 6.1.

Table 6.1. Load quantities of IEC standard (Holierhoek, 2010)

Load quantities	Specification
Blade root loads	Flapwise and edgewise bending moments
Rotor loads	Tilt moment Yaw moment Rotor Torque
Tower loads	Tower base moments in two directions

In addition to the load quantities, meteorological and wind turbine operation quantities are considered by in the IEC standard 61400-13 in the load assessment of wind turbines (Holierhoek, 2010):

Meteorological quantities in the IEC standard 61400-13 (Holierhoek, 2010):

- Wind speed
- Wind shear
- Wind direction
- Air temperature
- Temperature gradient
- Air density

Turbine operation quantities in the IEC standard 61400-13 (Holierhoek, 2010):

- Electrical power
- Rotor speed
- Pitch angle
- Yaw position
- Rotor azimuth
- Grid connection
- Brake status
- Wind turbine status

It is expected that all these quantity lists are going to be updated in the next version of the IEC standard with additional parameters and/or quantities.

The load assessment requires calculation/simulation and their validations by full load measurement campaigns within the testing and certification phase. The load measurement procedures are usually expensive and without measuring standard load quantities, it is difficult to perform a load assessment by only analyzing standard wind turbine SCADA parameters.

The load monitoring of wind turbines are usually done during the design and testing phase and performed at site conditions limited to the test site conditions matching the IEC standard's wind turbine classes. The site assessment process assures that the specific site conditions do not exceed the conditions of the IEC classes of the chosen wind turbine. For certain sites, when the site conditions do not go into the three predefined categories, the class S is introduced used where the turbines are adjusted to the site conditions. This usually requires specific load assessment by the wind turbine manufacturers.

The continuous load monitoring is not a default procedure in wind turbine operation. If it can be performed in a cheaper and simpler way, it can provide very valuable information. Such as with monitoring of fatigue loads, the reassessment of lifetime of the turbines can be performed, therefore a reduction in cost of energy can be achieved.

A detailed methodology proposed by Cosack (Cosack, 2010) with focus on fatigue load monitoring with standard wind turbine signals. He also presented a good literature overview of the load monitoring topic in 2010. In this thesis, Cosack investigated the connection between the loads and standard signals available from the wind turbines. He used inflow and turbine properties to categorize the load data and investigate their effects on loads. He also performed simulations and compared the results with actual measurements from several wind turbines. Cosack applied artificial neural network (ANN) technique to estimation of loads successfully. In addition to neural networks he has also summarized other techniques as transfer functions (Cosack, 2010):

1. Regression techniques
2. Neural networks
3. Physics-based models
4. State estimators

In his master thesis, Koopman (Koopman, 2013) built upon Cosack's research. He also provided a literate overview of load monitoring of wind turbines. He cited to notable works such as ECN's flight leader concept which aimed load assessment of a wind farm using ANN technique based on limited number of turbine's SCADA data by Obdam et al (Obdam, 2009). Koopman has focused on a physical approach model to monitor fatigue loads. By using the acceleration of the tower top, first tower top deflection found with double integration of acceleration and then tower bending moment is found using a beam model.

There is limited number of load monitoring research and techniques available in wind energy and there is still room for development in this field. A recent methodology developed by Svenningsen et al (Svenningsen, 2015) gives an alternative approach to load assessment. This method, so called Load Response and has become a module of WindPRO software (EMD International A/S, 2015), compares the site specific conditions with the pre-calculated response surface method (RSM) based on load simulation either on a generic turbine or a specific turbine. At the time being Load Response covers the fatigue loads during power production only, so the extreme loads are not covered. The site parameters used in Load Response are effective turbulence, wind shear, inflow angle and air density.

Based on the combination of these parameters first loads are calculated from the response surface. The resultant damage equivalent fatigue loads are calculated using Wöhler exponent (S-N curve) by combining all load components and at last the number of load cycles is compared to ones limited by design lifetime of the turbine.

LOAD MONITOR 1

The aim is to increase our knowledge on how climate, terrain and forest conditions corresponding to those of Sweden affects the performance of, and loads on a wind turbine.

Key achievements are:

- The development of a portable device that measures vibrations in the nacelle that can be used to derive approximate time evolution of loads.
- The indication that the production efficiency strongly depends on the atmospheric stability in such a way that increased atmospheric stability decrease the production efficiency. At the LoadMonitor site, suppressed turbulence with increased atmospheric stability seems to be the major reason for the relationship.
- A modified flow-model, which represent non-homogenous local variations in the canopy and terrain, and are able to reproduce the observed wind conditions. The fact that the flow model can reproduce the wind field over forest is a large step towards an accurate computation of wake interactions inside onshore windfarms.

Energiforsk is the Swedish Energy Research Centre – an industrially owned body dedicated to meeting the common energy challenges faced by industries, authorities and society. Our vision is to be hub of Swedish energy research and our mission is to make the world of energy smarter! Vindforsk is operated in cooperation with the Swedish Energy Agency.

Energiforsk Energimyndigheten